NAVAL POSTGRADUATE SCHOOL

MONTEREY, CALIFORNIA

THESIS

A DESCRIPTION OF THE CURRENTS ON THE CONTINENTAL SHELF NEAR EEL POINT, SAN CLEMENTE ISLAND, CALIFORNIA, FROM JULY 10, 2006, TO JULY 23, 2007

by

Cristal C Armijo

March 2008

Thesis Advisor: Curtis A. Collins
Co-Advisor: Fred Bahr

Approved for public release: distribution unlimited

THIS PAGE INTENTIONALLY LEFT BLANK

REPORT DOCUMENTATION PAGE			*Form Approved OMB No. 0704-0188*
Public reporting burden for this collection of information is estimated to average 1 hour per response, including the time for reviewing instruction, searching existing data sources, gathering and maintaining the data needed, and completing and reviewing the collection of information. Send comments regarding this burden estimate or any other aspect of this collection of information, including suggestions for reducing this burden, to Washington headquarters Services, Directorate for Information Operations and Reports, 1215 Jefferson Davis Highway, Suite 1204, Arlington, VA 22202-4302, and to the Office of Management and Budget, Paperwork Reduction Project (0704-0188) Washington DC 20503.			
1. AGENCY USE ONLY ***(Leave blank)***	**2. REPORT DATE** March 2008	**3. REPORT TYPE AND DATES COVERED** Master's Thesis	
4. TITLE AND SUBTITLE A Description of the Currents on the Continental Shelf Near Eel Point, San Clemente Island, California, from July 10, 2006, to July 23, 2007.			**5. FUNDING NUMBERS**
6. AUTHOR(S) Cristal C Armijo			
7. PERFORMING ORGANIZATION NAME(S) AND ADDRESS(ES) Naval Postgraduate School Monterey, CA 93943-5000			**8. PERFORMING ORGANIZATION REPORT NUMBER**
9. SPONSORING /MONITORING AGENCY NAME(S) AND ADDRESS(ES) N/A			**10. SPONSORING/MONITORING AGENCY REPORT NUMBER**
11. SUPPLEMENTARY NOTES The views expressed in this thesis are those of the author and do not reflect the official policy or position of the Department of Defense or the U.S. Government.			
12a. DISTRIBUTION / AVAILABILITY STATEMENT Approved for public release; distribution is unlimited			**12b. DISTRIBUTION CODE**

13. ABSTRACT (maximum 200 words)

This thesis investigated the current patterns around San Clemente Island, California. The data were from a mooring located at Eel Point, during the period July 10, 2006 to July 23, 2007. The currents were dominated by strong poleward flow along isobaths. Semi-diurnal and diurnal tides dominated the kinetic energy and rotary spectra. Clockwise rotation dominated the rotary spectra with inertial peaks in both the near surface and near bottom depths. There were on average 2-3 current reversals every three months which appear to be unrelated to the wind stress curl. The stratification was described for the year, with one upwelling event occurring in late spring. Using wavelet analysis, it was shown that inertial/diurnal and semi-diurnal energy were present intermittently throughout the water column. The strongest modes of energy were associated with the near bottom depths. Wind stress was poorly related to the currents.

Oscillations with a 2-3 day period were observed in the alongshore flow. These lasted for approximately 10 days in April 2007 and are referred to as the April event. This event was observed from mid-water to the bottom. The event had maximum velocities of 30 cm/s at mid-water and upward phase speed of 0.12 cm/s. These oscillations were rectilinear at mid-water and became counter clockwise with depth. It is speculated that this event may have been a coastally trapped wave but, with these data it cannot be determined as such.

SCI/SCORE is owned and operated by Navy and supports training for the largest concentration of naval forces in the world. This thesis provides information on ocean currents and stratification on the continental shelf at SCI for SCORE and military participants to use with military exercises, regional climatologies, ocean engineering design studies, and marine mammal studies.

14. SUBJECT TERMS SCORE, San Clemente Island, tidal, wavelet, spectra, Eel Point, mooring, currents, Southern California, inertial, diurnal, semi-diurnal, coastally trapped wave			**15. NUMBER OF PAGES** 101
			16. PRICE CODE
17. SECURITY CLASSIFICATION OF REPORT Unclassified	**18. SECURITY CLASSIFICATION OF THIS PAGE** Unclassified	**19. SECURITY CLASSIFICATION OF ABSTRACT** Unclassified	**20. LIMITATION OF ABSTRACT** UU

NSN 7540-01-280-5500

Standard Form 298 (Rev. 2-89)
Prescribed by ANSI Std. 239-18

THIS PAGE INTENTIONALLY LEFT BLANK

Approved for public release; distribution is unlimited

A DESCRIPTION OF THE CURRENTS ON THE CONTINENTAL SHELF NEAR EEL POINT, SAN CLEMENTE ISLAND, CALIFORNIA, FROM JULY 10, 2006, TO JULY 23, 2007

Cristal C Armijo
Lieutenant, United States Navy
B.S., Old Dominion University, 2001

Submitted in partial fulfillment of the
requirements for the degree of

MASTER OF SCIENCE IN METEOROLOGY AND PHYSICAL OCEANOGRAPHY

from the

NAVAL POSTGRADUATE SCHOOL
March 2008

Author: Cristal C. Armijo

Approved by: Curt A. Collins
Thesis Advisor

Fred Bahr
Co-Advisor

Mary L. Batteen
Chairman, Department of Oceanography

Phil Durkee
Chairman, Department of Meteorology

THIS PAGE INTENTIONALLY LEFT BLANK

ABSTRACT

This thesis investigated the current patterns around San Clemente Island, California. The data were from a mooring located at Eel Point, during the period July 10, 2006 to July 23, 2007. The currents were dominated by strong poleward flow along isobaths. Semidiurnal and diurnal tides dominated the kinetic energy and rotary spectra. Clockwise rotation dominated the rotary spectra with inertial peaks in both the near surface and near bottom depths. There were on average 2-3 current reversals every three months which appear to be unrelated to the wind stress curl. The stratification was described for the year, with one upwelling event occurring in late spring. Using wavelet analysis, it was shown that inertial/diurnal and semidiurnal energy were present intermittently throughout the water column. The strongest modes of energy were associated with the near bottom depths. Wind stress was poorly related to the currents.

Oscillations with 2-3 day period were observed in the alongshore flow. These lasted for approximately 10 days in April 2007 and are referred to as the April event. This event was observed from mid-water to the bottom. The event had maximum velocities of 30 cm/s at mid-water and an upward phase speed of 0.12 cm/s. These oscillations were rectilinear at mid-water and became counterclockwise with depth. It is speculated that this event may have been a coastally trapped wave but, with these data it cannot be determined as such.

SCI/SCORE is owned and operated by Navy and supports training for the largest concentration of naval forces in the world. This thesis provides information on ocean currents and stratification on the continental shelf at SCI for SCORE and military participants to use with military exercises, regional climatologies, ocean engineering design studies, and marine mammal studies.

THIS PAGE INTENTIONALLY LEFT BLANK

TABLE OF CONTENTS

THIS PAGE INTENTIONALLY LEFT BLANK

LIST OF FIGURES

THIS PAGE INTENTIONALLY LEFT BLANK

LIST OF TABLES

THIS PAGE INTENTIONALLY LEFT BLANK

ACKNOWLEDGMENTS

I would like to acknowledge my advisor Professor Curt Collins and co-advisor Fred Bahr with a sincere thanks for their patience, knowledge, and guidance. I would also like to thank Fred for all the countless hours helping me with MATLAB®. I want to extend a special thanks to the following: Professor Jeff Paduan for helping me with some of my data interpretation and analysis. Tetyana Margolina for running the wavelet analysis with my data set, and also helping me interpret the results. Marla Stone for creating the mooring diagram and helping me with some initial processing. Additionally, Tarry Rago for creating the mooring location picture for my poster and thesis.

Most importantly, I want to thank my family for always encouraging and believing in me, especially my Mom.

THIS PAGE INTENTIONALLY LEFT BLANK

I. INTRODUCTION

Current and future naval operations are focused on coastal/littoral regions around the world. An accurate description of current variability is important to the Navy for a number of reasons, such as: mine-hunting, acoustic propagation, search and rescue, dispersion, small boat, amphibious and special operations. The United States Navy has owned, operated and trained on San Clemente Island, California since 1934. The Southern California Offshore Range (SCORE) is a division of Naval Air Force Pacific and is currently assigned operation control for all operations in and around San Clemente Island. The SCORE provides tactical range training and testing services to U.S. Navy units of the Pacific Fleet. The purpose of this study was to analyze and describe the coastal current variability on the continental shelf near Eel Point, San Clemente Island (SCI). SCI located in the Southern California Bight (SCB) region, 75 miles northwest of San Diego, California.

A year of data from an ongoing study was collected in order to observe the currents near Eel Point. A mooring (Fig. I-1) was located in about 130 m on the continental shelf at 32º 55' N, 118º 35' W. The objective was to gain a better understanding of current variability and stratification along the shelf of SCI. Due to Navy training exercises there have been few studies conducted at this location. This study investigates the physical forcings which may have played a role in driving the currents. Little is known about the circulation patterns around SCI and what is driving them. There are several studies which attempt to correlate the wind stress and ocean currents within the SCB (Winant and Dorman, 1997; Hickey, 1998; Bray et al., 1999; Hickey et al., 2003). Winds are a major driving force of the currents. This study attempts to relate wind stress and wind stress curl to the currents. This study will first describe the energy associated with the raw currents by calculating the principal axis of rotation, spectral analysis (kinetic energy and rotary spectra), and tidal analysis. In order to investigate the seasonal variability, the data set was divided into seasonal 3 month segments to describe the vertically averaged currents, along and cross-shore components,

and stratification throughout the water column. A wavelet analysis was run using the baroclinic currents and wind stress (calculated from three NDBC buoy stations, discussed later). The curl of the wind stress was calculated and then compared to the alongshore currents in an attempt to explain the current reversals observed throughout the time-series. A simple slab model following Pollard and Millard (1970) was used to investigate the oscillations observed in the currents.

A. LITERATURE REVIEW

1. Large Scale Circulation

The large-scale ocean circulation that occupies the Northern Pacific basin is known as the North Pacific Subtropical Gyre. It is has a dominant anticyclonic flow which is comprised of four currents systems: the North Pacific Current to the north, California Current to the east, North Equatorial Current to the south and the Kuroshio Current to the west. The dominant patterns of the atmospheric circulation that drive the California Current System (CCS) are the North Pacific High, the Aleutian Low and in summer the thermal low over the southwestern United States. SCORE is located with the California Current System.

2. California Current System

The California Current System (CCS) is an eastern boundary current system that runs along the west coast of North America from the Strait of Juan de Fuca to the tip of Baja California. The CCS is comprised of the equatorward-flowing California Current (CC); the poleward-flowing Davidson Current (DC), the poleward-flowing California Undercurrent (CU), and the Southern California Eddy (SCE). Seasonal variations in alongshore wind stress, coastline irregularities, bottom topography, and stratification, have been shown to be the mechanisms responsible for the observed large-scale structure within the CCS (Hickey, 1998).

The CC is a slow (~2-10 cm/s), broad (~1000 km), equatorward year-round surface current. It carries colder, fresher subarctic water equatorward along the west

coast (Hickey, 1998). The current is strongest at the sea surface and generally extends over the upper 500m of the water column. The CC has a seasonal maximum in summer to early fall (Hickey, 1998) and is linked with seasonal jets and eddies. South of Point Conception, Lynn and Simpson (1987) use dynamic height fields to show the CC turns eastward, flowing into the Southern California Bight at 32º N. The eastward flow creates a cyclonic gyre (Southern California Eddy) within the bight that is strongest in late summer and fall.

The CU is a narrow (~10-40 km) and relatively weak (~2-10 cm/s) current that flows poleward over the continental slope from Baja California to at least Vancouver Island (Hickey, 1998). The current is strongest at depths of ~100-300 m from the surface. It transports warmer and saltier subtropical waters poleward. Hickey (1979) concluded that the location, strength and core depth have shown considerable seasonal variability which can be related to the seasonal variability in wind stress and wind stress curl. It has seasonal maxima in late spring and summer with peak speeds of ~30-50 cm/s (Hickey, 1998).

The DC flows poleward in the fall and winter from (~35º N) Point Conception to Vancouver Island (~50º N) (Hickey, 1998). It is a relatively broad (~200 km) and, weak (~5 cm/s) surface current. The DC seasonal maximum is in the winter. In Huyer et al. (1989), the reversal of winds from northwesterly in the summer to southeasterly in winter caused downwelling at the coast. This may be one of the forcing mechanism of the poleward flowing surface current known as the Davidson Current (Huyer et al., 1989).

3. Circulation in the Southern California Bight

The Southern California Bight (SCB) has a concave curvature between the headland at Point Conception and the U.S.-Mexican border (Lynn and Simpson, 1990). Due to the SCB's complex bathymetry, it is considered to be a difficult region to determine seasonal circulation patterns. The bight is punctuated by a series of complex topographic features such as islands, basins and ridges. These exert strong control on circulation patterns at every depth and are governed by seasonal patterns in the CCS (Hickey, 1979, 1998, Lynn and Simpson, 1990; Bray et al., 1999, Hickey et al., 2003).

The CC flows equatorward offshore of the bight. A portion of the CC turns inshore and poleward, it then recirculates within the bight forming the Southern California Countercurrent (SCC). This circulation pattern has been referred to as the Southern California Eddy (SCE) (Figure I-2). The SCE is strongest in summer and early fall and weakest or even non-existent in spring (Hickey et al., 2003). The poleward flowing California Undercurrent (CU) lies beneath the sea surface (~100-200 m core depth) and is a dominant feature of circulation in the bight (Hickey et al., 2003).

Spring and summer winds off Point Conception are strong due to the large pressure gradient between the North Pacific high and the thermal low over the southwest U.S. (Winant and Dorman, 1997). During the fall and winter, the atmosphere is dominated by traveling cyclones and anticyclones. Winds within the SCB (near the coast) are generally weak and directed onshore during the spring and summer. During the summer, the dominant wind direction is equatorward along the coast. This pattern is mostly influenced the by the North Pacific High. However in the winter it tends to reverse direction along northern California. Maximum equatorward wind stress occurs during the spring in southern California, and during late fall summer in northern California. Minimum equatorward stress occurs during late fall and winter (Hickey, 1998).

B. THESIS ORGANIZATION

For this study, a one year period of ocean current observations from July 10, 2006 to July 23, 2007 were used. The location of the of mooring site was near Eel Point which is located on the west coast of San Clemente Island (SCI), California. This thesis is the first to describe the current variability at this site. We will look first at the variability and stratification within the water column on the continental shelf (Eel Point mooring). Data collection will be discussed chapter II. Description of the currents and data analysis will be discussed chapter III. Chapter IV discusses the summary of results from the data analysis. Conclusions, future recommendations and Navy relevance are discussed in Chapter V.

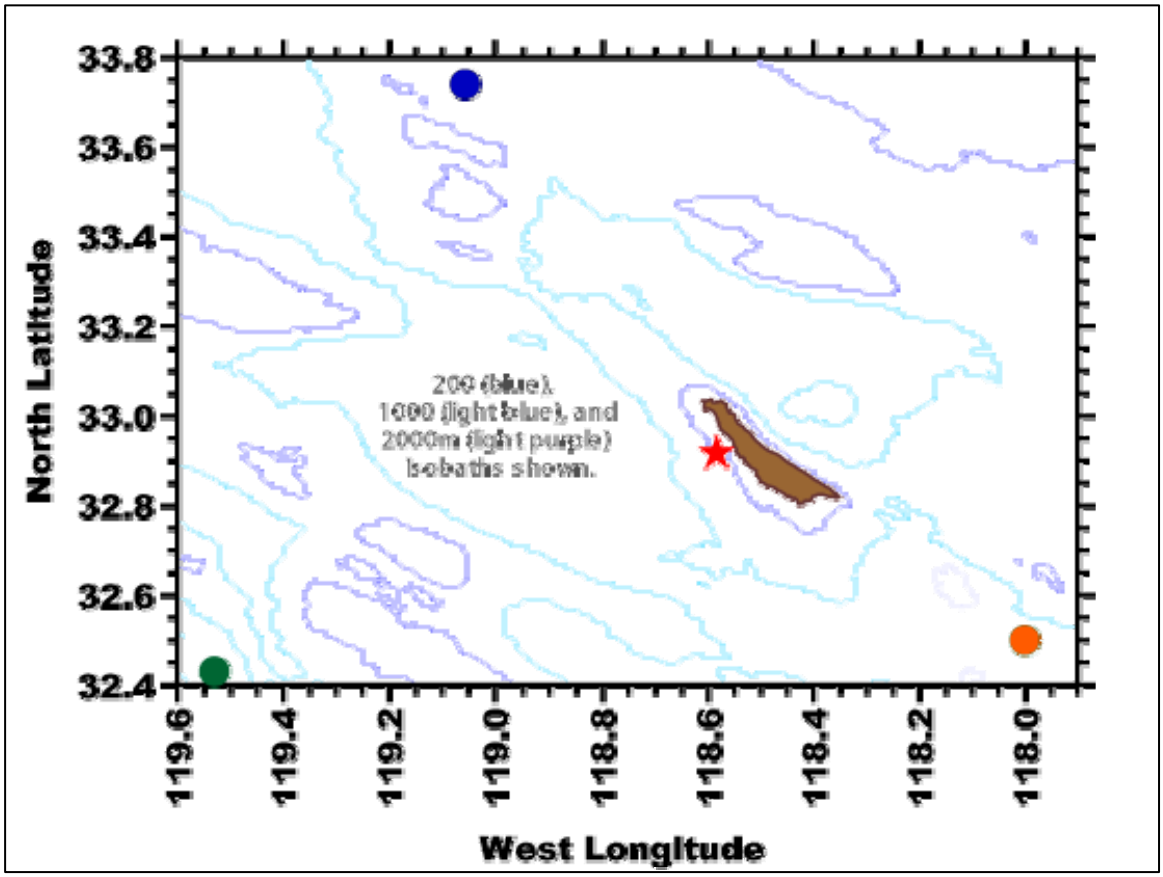

Figure I-1. San Clemente Island, California and the position of Eel Point Mooring (red star) and NDBC stations 46025 (SMB-blue dot), 46047 (TB - green dot), 46086 (SCB – orange dot).

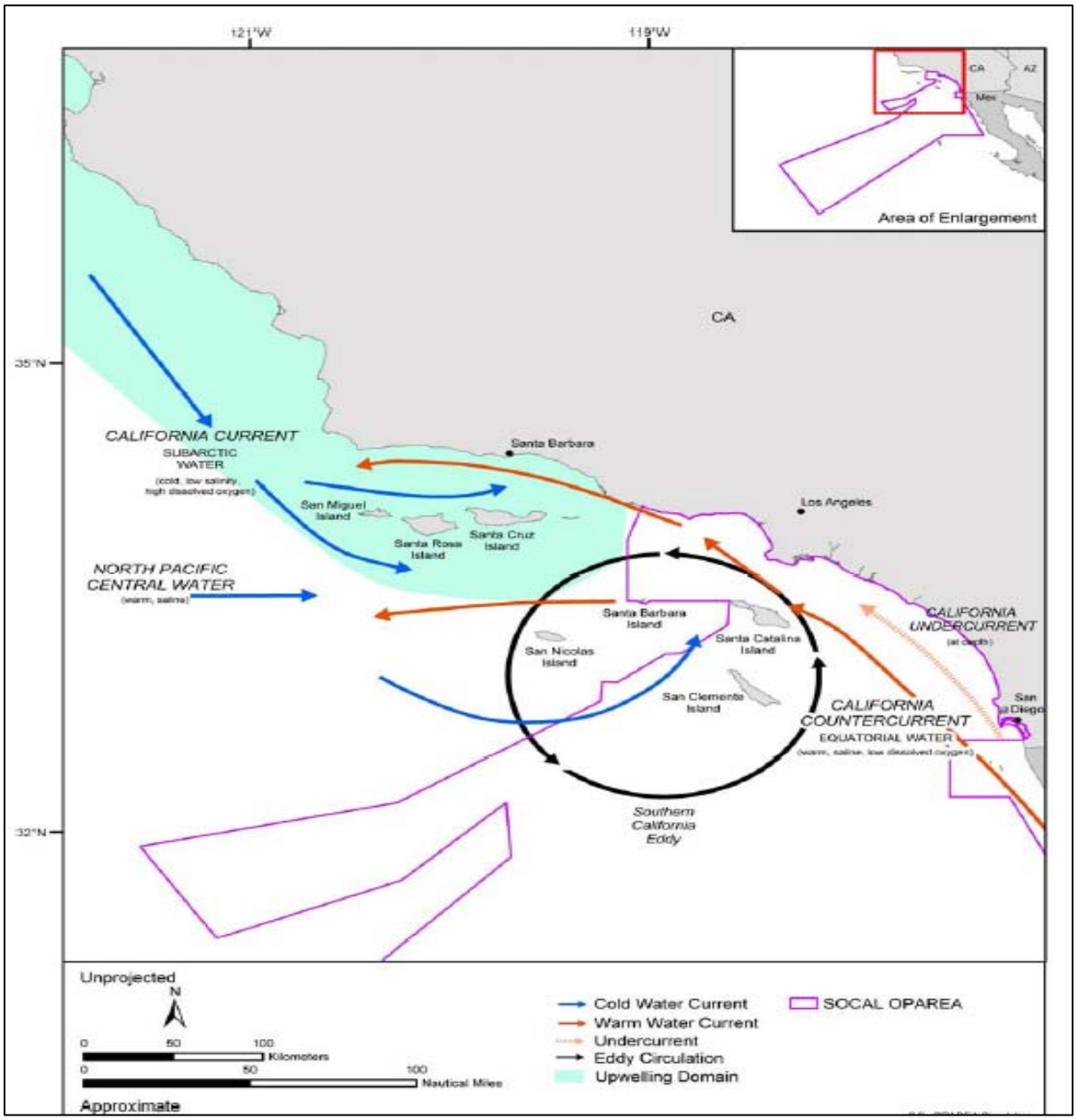

Figure I-2. Major currents affecting the circulation of the SOCAL OPAREA. (Department of the Navy, 2005)

II. DATA COLLECTION

This chapter will describe data collection and processing for the moorings at Eel Point, San Clemente, California (Figure II-1). The Eel Point mooring data used for this study consisted of two consecutive 6-month deployments SCORE 2 (SC2) and SCORE 3 (SC3). This created a year long time-series. Data were collected by an upward-looking RD Instruments WorkHorse 300 kHz broadband Acoustic Doppler current profiler (ADCP) and three Sea-Bird Electronics SBE 37-IM MicroCATs. The Naval Postgraduate School (NPS) Oceanography Department and the Research Vessel *Point Sur* (*R/V Robert Gordon Sproul)* were responsible for deploying and (recovering) the moorings in July 2006 (January 2007). SC3 was recovered by *R/V Point Sur* on July 23, 2007.

A. EEL POINT MOORING (SC2 AND SC3)

The Eel Point mooring was located on the west coast of SCI. Its location was chosen in consultation with NPS and SCORE so as to not interfere with naval training activities. Deployments of the mooring began in January 2006 with (SC1). For this study, we will use the data from deployments SC2 and SC3. SC2 was deployed on July 10, 2006 at 32° 55.718'N, 118°36.503'W and recovered on January 18, 2007. The bottom depth at the mooring was 130 m. A 300 kHz ADCP was deployed at a depth of 118 m on the mooring. Three MicroCATs were also deployed on the mooring at depths of 40 m, 80 m, and 118 m. SC3 was deployed on January 18, 2007 at 32º 55.805'N and 118º 35.676'W and recovered on July 23, 2007. The bottom depth at the mooring was 135 m. The ADCP was deployed at 120 m. The three MicroCATs on this deployment were at 45 m, 85 m, and 123 m. Both deployments will be referred to as the Eel Point Mooring. Prior to the deployments, the ADCP and the MicroCATs were calibrated and tested by the NPS Oceanography Department.

The instruments (ADCPs and MicroCATs) used to collect data at the Eel Point mooring were not set to sample at the same rate. The ADCP sampled every 15 minutes

and the MicroCATs sampled every 5 minutes. The RDI WorkHorse broadband ADCP uses an acoustic pulse and the Doppler shift principle to measure current velocities throughout the water column. The ADCP transmits an acoustic signal (a "ping") at a fixed frequency of 307.2 kHz. The transducers listen for the return echo from the backscatters in the water. The ADCP uses a four-beam transducer head with a 20 degree beam angle. In order to calculate the current velocities using a multiple beam solution, the ADCP assumes the currents are homogeneous throughout the horizontal water plane. Trigonometric and geometric relations between the beams are used to calculate the three-dimensional current velocity vectors. These are the u (north-south), v (east-west), and w (up-down) components. The fourth beam is a redundant beam used to calculate the error velocity and to the check the assumption of horizontal homogeneity. Error velocity is the difference between a velocity measured by one set of three beams versus a velocity measured by the other set of three beams during the same time frame (Simpson, 2001). Large differences could be associated with a non-homogenous environment or corrupt data caused by a large fish or obstruction blocking the transmission of the signal.

The ADCP was setup with 4 m bin spacing and measures the average velocity over the depth range of each depth cell to produce a current velocity profile. Averaging over the range of each depth cell reduces the affects of spatial aliasing (Gordon, 1996). The profiles are generated by range-gating the echo signal (Gordon, 1996). Because shorter ranges return the echo signal faster than longer ranges, range gating was developed to break the received signal into successive segments for independent processing (Gordon, 1996). The ADCP was configured to burst sample. The burst sample consisted of 40 consecutive one-second pings during the initial 40 seconds of the 15 minute ensemble time. Burst sampling was used to prevent aliasing of surface wave velocities. Sampling the first 40 seconds enabled the ADCP to measure the entire surface wave/swell cycle. By taking the average of this sample, the ADCP captured the true current velocity without significant bias caused by surface waves.

Echo intensity is scaled, using about 0.45 decibels per WorkHorse count. It is a measure of signal strength. For the upward-looking ADCP, echo intensity is important. Echo intensity and the signal-to-noise ratio decrease with range. With increasing range

the echo intensity signal begins to weaken and flatten out. If a rapid increase (spike) in the echo intensity is observed, it is most likely due to the transducer's signal side lobe having been reflected by the ocean surface and that the side lobes of the acoustic pulse are contaminating the velocity signal. Two criteria were used to flag bad data from the ADCP. For this study, once the echo intensity flattened out for several successive bins and then a spike in intensity occurred, it was then safe to assume that the ADCP stopped collecting good data. By comparing the echo intensity to the correlation magnitude, if both values fall below 64 counts then the data are flagged as bad. The second criterion is based on the three and four beam solution. If the percent good values of the 3 and 4 beam solutions were less than 25% then the data are flagged as bad.

In order to have one continuous year long time-series, SC 2 and SC 3 were patched together. There was a 2 hr 45 min. gap in time between deployments. The gap was first filled with NaN's (not-a-number). For the spectral analysis, these were replaced with zeros. Time-series used for spectral analysis can not have NaNs or gaps. The bin depth values for each deployment were compared and matched with the closest single array of common mutual depth. The center of the lowest bin that was common to both deployments was 118 m and highest common usable bin was at 26 m. There were a total of 24 bins.

The SBE 37-IM MicroCAT recorded conductivity, pressure and temperature. Temperature was measured by applying an alternating current to an airtight VISHAY reference resistor and an ultra-stable aged thermistor. Salinity was a derived from the conductivity and temperature measurements. Each mooring had three MicroCATs that sampled every 5 minutes. For the 1-year period the sampling depths were set to 50 m, 91 m and 129 m. Portions of the conductivity data appeared to be offset, probably due too material in the cell; salinity for these periods were estimated using the T-S relationship as determined by good data.

B. WINDS

Wind data were downloaded from "NOAA's National Data Buoy Center" (NDBC), http://www.ndbc.noaa.gov. Historical wind data were used from Stations 46086, (San Clemente Basin, SCB), 46047, (Tanner Banks, TB), and 46025, (Santa Monica Basin, SMB). The period of time used was the same as the time-series. However, there was a data gap from May 10, 2007, until June 18, 2007, due to a failure in the anemometer at the SCB buoy (see Figure I-1 for reference location of the buoys in relation to the SCI).

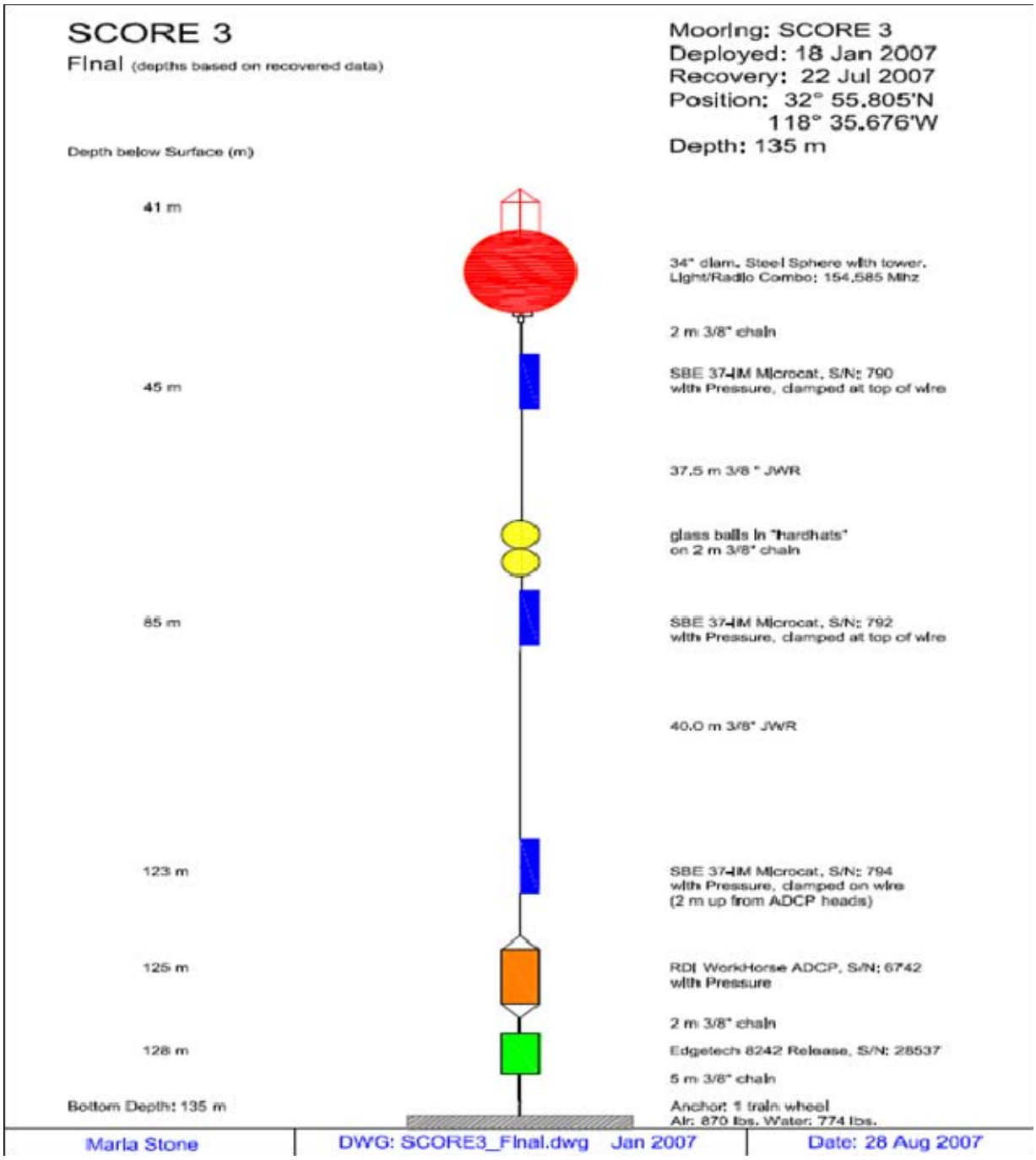

Figure II-1. Schematic diagram of the mooring at Eel Point. The same configuration was used for both SCORE 2 (SC2) and SCORE 3 (SC3). SC2 bottom depth: 130 m and SC3 bottom depth: 135 m.

THIS PAGE INTENTIONALLY LEFT BLANK

III. DATA ANALYSIS METHODS

A. INITIAL PROCESSING

The ocean currents, temperature and salinity data collected from the ADCPs and MicroCATs for Eel Point were broken into different files for separate processing and clean up. Raw ADCP data were processed using the MATLAB® program Workhorsepro1 (written by Prof. Curt Collins) designed to flag and remove bad data points and interpolate with replacement values. The resulting time-series was then despiked and a linear interpolation was again used to replace the extreme values. These cleaned up interpolated data will henceforth be referred to as the raw data. Rotated, filtered, and vertically averaged data files were created for future use. The filter used to smooth the currents, and stratification (T-S) data was a 4^{th} order low-pass Butterworth filter, the nondimensional cutoff frequency used for the currents was .01 and the cutoff for the T-S was .0035 (the cutoff values are different in order to compensate for the different sample rates), these values equate to an ~50 hour low-pass filter (50lp). This was used to remove the tidal frequencies from the data. All data analyses were processed using tailored MATLAB® programs.

B. UNSMOOTHED CURRENT OBSERVATIONS

It was necessary to first analyze the raw data at all depths, in order to gain an idea of the vertical structure of the flow. Table 1 contains the mean, maximum, minimum and the standard deviation of the current velocity for the U and V components at each bin depth. The mean current flow was a dominant poleward flow in the V component and a dominant westward flow in the U component. The maximum (minimum) V component was recorded at 46.7 cm/s (-80.2 cm/s) and the U component was 61.1 cm/s (-58.4 cm/s).

Histograms of speed and direction for the (unsmoothed) raw currents recorded by the ADCP at a 15 minute sample intervals for the near surface (34 m), middle water column (74 m), near bottom, and vertically averaged currents are shown in Figures III-1.

The speed and direction bin sizes used in the histogram were 0.5 cm/s and 1˚. At the near surface, the most frequently observed current speed was 7.5 cm/s with a maximum current speed of 50 cm/s and most frequently observed direction of 333˚ T. In the middle water column, the most frequently observed current speed was 5.5 cm/s with a maximum current speed of 50 cm/s and most frequently observed direction of 337˚ T. In the near bottom currents, the most frequently observed current speed was 5.5 cm/s with a maximum speed of 44 cm/s and most frequently observed direction of 342˚ T. The most frequently observed current speed for the vertically averaged flow was 4 cm/s with a maximum speed of 37 cm/s and most frequently observed direction of 338˚ T. The histograms showed the predominant flow to be northward along the isobaths. The local isobaths were oriented at 330˚ T.

C. PRINCIPAL AXES

The ADCP data were rotated into their principal axes. The rotation maximizes the variance along the major axis and minimizes it along the minor axis. The major axis is now referred to as the alongshore component and the minor axis is the cross-shore component. The orientation of the principal axis, θ is determined by (Emery and Thomson, 1997):

$$\theta = \frac{1}{2}\tan^{-1}\left[\frac{2\langle u'v'\rangle}{\langle u'^2\rangle - \langle v'^2\rangle}\right],$$

Where $u' = u - \overline{u}$ and $v' = v - \overline{v}$. In the new coordinate system, the rotated velocity components are defined as

$$u_r = u'\cos\theta + v'\sin\theta$$

and

$$v_r = -u'\sin\theta + v'\cos\theta.$$

In this coordinate system, the maximum variance is associated with v_r which represents the alongshore (major axis) component, while the orthogonal component (minimum variance) is associated with u_r the cross-shore (minor axis) component. The purpose of the principal axes were to determine the orientation of the variability of the flow and

decompose the velocity into uncorrelated scalar components (Emery and Thompson, 1997). It also gives a statistical picture of the variance for a set of vector time-series (Table 2).

For this study the principal axis rotation was calculated using a MATLAB® function, princax (written by Rich Signell). This function calculates θ (angle of maximum variance) in mathematical coordinates (90 is north and 0 east). An example for the vertically integrated flow is shown in a scatter plot (Figure III-2). For the example, θ = -55˚ (-55 subtracted from 90 gives 145 + 180 = 325). The alongshore direction is now orientated along 325º T to 145º T, and cross-shore 235º T to 55º T. The alongshore orientation aligned very closely with the topography. For example, NOAA chart 18762 indicated that the isobaths were oriented along 330 º at the mooring location.

D. SEASONAL VARIABILITY

The bight region is a complex environment which has high temporal and spatial variability due to the local winds in addition to the eight nearshore islands, submarine canyons, ridges, and basins which disrupt the large scale circulation. This section describes of the seasonal variability of currents (vertically averaged over 24 bin depths between 26 m and 118 m) and temperature and salinity at the Eel Point mooring. The current velocity, temperature and salinity data used were divided into 3 month seasonal segments, starting with summer (July 10, – September 30, 2006), fall (October 1, - December 31, 2006), winter (January 1, - March 31, 2007) and spring (April 1, - June 30, 2007). The data used to create all figures in this section were rotated and lowpass filtered (previously described) to remove the tidal variability.

1. Summer

In the summer, the vertically averaged currents (Figure III-3) show fairly weak alongshore currents which are predominantly poleward flowing. However there are 3 short current reversals. The cross-shore currents are very weak and flow toward the island until the end of August when a significant increase in current velocity (15 cm/s) along with a flow reversal offshore occurs for about 15 days. The contour plots (Figures III-4)

show the current velocities with depth. The contours are consistent with the vertically averaged currents and show that the cross-shore reversals penetrate throughout the water column, but were stronger at the surface and weaken toward the bottom.

The summer temperature time-series (Figure III-5) shows a significant difference in temperature between 50 m and 91 m, ΔT averaging 3˚ C between these depths. At 50 m, the temperature steadily rose to a maximum of 14.3˚ C and maximum ΔT of 4.5˚ C between depths 50 m and 129 m in mid-September. Temperatures at 91 m and 129 m increased little. For summer salinity (Figure III-5), the salinity increased with depth compared to temperature which decreased with depth. This figure shows that salinity and temperature were inversely proportional to each other.

2. Fall

The vertically averaged currents in the fall (Figure III-6) start off weak with 3 small reversals in current flow in the alongshore and cross-shore flow. By mid-November the alongshore flow increases and is predominantly poleward in direction and the cross-shore flow increases eastward (toward the island). In the fall, contour plots (Figure III-7) of the alongshore flow and cross-shore flow almost mirror each other. When the alongshore flow is poleward the cross-shore flow is eastward.

The fall temperatures (Figure III-8) were slightly warmer than the summer at 50 m with a maximum peak 15.1˚ C and maximum ΔT 5˚ C at end of October. After the maximum peak, the temperatures decreased and averaged between 13-14˚ C. There was a significant decrease in ΔT= 2.2˚ C between 50 m and 91 m. There were variations at 50 m which did not propagate down through the water column. There were no significant variations in the salinity time-series (Figure III-8). The relative stratification between the layers, remain constant, until late December when more mixing was observed between the layers.

3. Winter

The winter vertically averaged currents (Figure III-9) show a fairly strong and predominantly alongshore poleward flow. At the beginning of February, there was an

onset of a strong equatorward reversal lasting for 10 days. The cross-shore flow fluctuated at the beginning of January. It then remained relatively weak throughout the season. The winter alongshore contour plot (Figure III-10) shows that the oscillations and reversal observed in the vertically averaged currents do penetrate down through the water column, with maximum velocities observed at mid-depths. In the cross-shore the eastward flow was uniform throughout the water column.

The winter temperatures (Figure III-11) were the warmest at all depths in comparison with the other seasons. At 50 m there were a lot of variations in temperature. The maximum temperature peak was 14.8˚ C with a max ΔT 4.8˚ C between the depths. At 91 m and 129 m the temperatures were 1-2˚ C warmer than summer and fall. The winter salinity time-series (Figure III-11) shows less stratification between the 50 m and 91 m, meaning there was more mixing between the two depths.

4. Spring

The spring vertically averaged currents (Figure III-12) show the strongest (23 cm/s) poleward alongshore flow. The cross-shore flow was relatively weak and directed eastward. Starting around April 10th the alongshore flow showed an oscillation with a 2-3 day period which lasted about 10 days (hereafter, referred to as the April event). The oscillation can be seen in the contour plot (Figure III-13): the current velocities were strongest at mid-depth. The vertical phase change for the April event was estimated to be 0.12 cm/s, (Δz = 40 m determined for a 2 day period (April 15 – 17, 2007).

In the spring temperature and salinity time-series (Figure III-14), the April event (oscillation) was observed at all depths. The temperature steadily decreased with time at all depths. The largest temperature difference was observed at 50 m, decreasing from 14.1˚ C to 11.4˚ C (ΔT=2.7˚ C). At 91 m and 129 m the temperature steadily decreased to < 10˚ C. The salinity stayed relatively stratified throughout the water column until early June when it increased, weakening the stratification. The observed cooler temperatures and saltier water characteristics are mostly likely the result of upwelling.

5. Recap of Seasonal Variation for the Year

Looking at the entire time-series, there were many 2-3 and 3-4 day patterns of oscillations observed in the current velocity and stratification. However, there were no discernable patterns over the whole year. Summer had the weakest observed currents. Winter and spring had the strongest currents. Winter had the warmest temperatures and spring had a cooling trend along with the coldest observed temperatures. Stratification was strongest throughout the summer and weakest at the end of spring due to upwelling.

E. SPECTRAL ANALYSIS

Spectral analysis is a way to show how the variance of a time-series varies as a function of frequency. Three types of spectra were calculated for this thesis, the kinetic energy, rotary, and wavelet spectra. The kinetic, rotary and wavelet spectra were computed using MATLAB® programs. The MATLAB® programs were based on the discrete fast Fourier transform (FFT) and the periodogram method. A Hanning window was applied with a 50% overlap. Prior to computing the spectrum, the record mean and trend were removed from the time-series. A 180 day piece length and a 95% confidence interval were used for both kinetic and rotary spectra.

1. Kinetic Energy Spectra

Kinetic energy (KE) spectra are a useful tool to study deterministic and stochastic processes. The Eel Point current time-series contained a mixture of both deterministic and stochastic processes. Deterministic processes are predictable, such as the tides, while stochastic processes are random, such as internal/inertial waves. The raw data were used to construct the KE spectra. The KE spectra were used specifically in this thesis to show the frequency of the dominant energy. Variance-preserving KE spectra were generated for three levels within the water column; 110 m, 74 m, and 34 m (Figure III-15). It showed that semi-diurnal and diurnal tides dominated the energy spectra. The semi-diurnal tidal energy was strongest at mid-water and weakest at the near-bottom. The diurnal tide was strongest at the near-surface and near-bottom. Knowing that the

dominant energy was in the semi-diurnal and diurnal frequencies, a band-averaged KE spectra at the same depths was created (Figure III-16), it confirms that the diurnal and semi-diurnal KE dominated the spectrum and that the semi-diurnal KE was about 20% greater than the diurnal KE.

2. Rotary Spectra

Rotary Spectra are used to separate the velocity vector frequency, ω, into clockwise and counterclockwise rotating circular components. The circular components replace the Cartesian components (*u*, *v*). The vector addition of the two oppositely rotating circular components cause the tip of the combined vector to trace out an ellipse over one complete cycle. If one of the two components equals zero, the motion is circular polarized, and if the two components are equal (same magnitude), then the motion is rectilinear (back and forth). In most cases, rotary spectral analysis has proven to be useful when investigating current variability. For the purpose of this thesis, rotary spectra were used to investigate inertial motions, diurnal frequency and any other types of oscillatory flow at the near-bottom (110 m), mid-water column (74 m), and near surface currents (34 m).

Figure III-17 shows that the clockwise energy was dominant over the counterclockwise energy at all three depths. The inertial frequency $\omega = 2\Omega \sin\phi$ was calculated using a latitude of 32˚, resulting in the inertial period $1/\omega$ = ~22.5 hours. At the near surface and near bottom the dominant peaks were at the diurnal, inertial and semi-diurnal. The mid-depth, the spectra did not contain the inertial peak.

F. TIDAL ANALYSIS OF CURRENTS

Tidal variability is often the largest signal of energy in a typical oceanic time-series (Pawlowicz et al, 2002). Tides are deterministic, meaning that they can be predicted and are mostly dominated by diurnal and semi-diurnal frequencies. Coastal environments such as the Southern California Bight region are highly dynamic in nature. The currents are often affected by deep ocean variability such as the tides which propagate through the shallower waters as a wave or combination of waves. In order to

understand the nature of the tidal currents, a harmonic (tidal) analysis was used to obtain the tidal constituents. The tidal analysis allows specific frequencies to be examined and amplitudes and phases to be estimated in a least-square sense (Emery and Thomson, 1997).

For this thesis, the Forman tidal harmonic analysis program was run using the MATLAB® code from Pawlowicz et al., (2002). The analysis uses the MATLAB® program T_TIDE to run the tidal analysis using the raw data. T_TIDE uses the least-squares method which is constrained to fit the frequencies that Forman specified as tidally important. The advantage of using the least-squares method is that it permits resolution of 67 tidal constituents (for this data set) of which 45 are typically astronomical in origin. Tables III-3 and III-4 list the five dominant constituents found using the tidal analysis. Further dynamical analysis requires the separation of the tidal effects from inertial effects. The semi-diurnal (M2) and diurnal (K1) tides were the dominant frequencies throughout the entire time-series, they were also very prominent in the KE spectra. The T_TIDE program creates a data file which contains all tidal constituents found at Eel Point mooring. The vertically averaged tidal constituents were computed and used to compute the predicted tides using the MATLAB® program T_PRED. The predicted tides were defined as the barotropic tidal currents. These barotropic tidal currents were used later in the wavelet analysis.

G. WAVELET ANALYSIS

Wavelet analysis is a good tool for localizing time-frequency information without requiring that the time-series be stationary. Wavelet analysis involves transforming a time-series into a series of coefficients that contain all the information of the original signal, which is similar to Fourier analysis. In a wavelet analysis, the signal is reconstructed by adding wavelets of different scales and at different translations together; as in a similar manner Fourier analysis reconstructs by adding sines and cosines of different periods together. The wavelet analysis optimally tiles the time-frequency domain allowing for dominant modes of variability to be determined and to distinguish how those modes vary in time.

For this analysis, the methods described in Torrence and Campo (1998) "Guide to Wavelet Analysis" and their toolbox were used to generate the wavelet spectra. Prior to computing the wavelet analysis, the record mean, trend, and barotropic tidal currents were removed from the time-series. A continuous wavelet transform which can use both orthogonal or nonorthogonal wavelet functions turns a signal into a function with two variables, scale and time. The basis function used was a Morlet wavelet which is the product of a complex exponential plane wave modulated by a Gaussian:

$$\psi_0(\eta) = \pi^{-1/4} e^{i\omega_0 \eta} e^{\eta^2/2},$$

where η is the nondimensional "time" parameter and ω_0 is the nondimensional frequency. In a wavelet power spectrum, different modes of energy are contoured in order to interpret how the amplitude of the signal changed with time and frequency. The wavelet function is normalized at each scale *s* to have unit energy. This unit energy criteria ensures that the wavelet transforms at each scale *s* are directly comparable to each other and other time-series. The normalization process takes place by using:

$$\psi\left[\frac{(n'-n)\delta t}{s}\right] = \left(\frac{\delta t}{s}\right)^{1/2} \psi\left[\frac{(n'-n)\delta t}{s}\right],$$

where *s* is the wavelet scale and *n* is the translation parameter. The factor of $s^{-1/2}$ indicates $\psi_0(\eta)$ has been normalized.

The Morlet wavelet was used for this analysis since it is particularly good at isolating periodic signals. The width of the wavelet function is defined in Torrence and Compo (1998) as the *e*-folding time of the wavelet amplitude. The resolution is determined by the wavelet scales. Small wavelet scales resolve the high frequency components, the wavelet itself is broad in frequency and the amplitudes of the peaks in the spectrum are smoothed out. The wavelets are scaled based on a relationship between the equivalent Fourier period. Because wavelets deal with finite length time-series, error will occur at the beginning and end of the wavelet power spectrum. One solution is to pad the end of the time-series with zeroes before computing the wavelet transform and then remove them afterward (Torrence and Compo, 1988). The cone of influence (COI)

is the area of the wavelet spectrum where edge effects become important. Outside the COI, estimates contain errors and may not represent the true period or energy.

For this analysis, Torrence and Compo (1998) software was used with the time-series padded with zeros. Ten suboctaves per octave (an octave is the difference between 2 frequencies that relate to each other by a factor of 2) were used to characterize the resolution in frequency. The highest resolved frequency corresponded to a period of 30 minutes and the lowest resolved frequency to 44 days for SC2 and SC3. The lowest resolved frequency for the 2 month segment was 20 days.

The barotropic tidal currents were subtracted from the rotated raw data to create the baroclinic tidal currents. The baroclinic tidal currents and the wind stress (discussed later) thus created were used in this wavelet analysis.

The wavelet analysis will look at SC2 and SC3 separately and then look at a smaller two month time segment. The same three depths used in the previous spectral analysis (34 m, 74, 110m) will also be the main focus of this analysis. The wavelet spectra depth figures represent the near-inertial/diurnal energy. They were created by averaging three different periods: 21.8, 23.4, and 25.1 hours which are not necessarily independent, estimates of wavelet power. SC2 alongshore and cross-shore wavelet components with depth (Figure III-18) show that the energy was only at the near surface and near bottom depths. In the middle of the water column (60-70 m) there was very little energy. SC2 (Figures III-19, 20, & 21) show that at all three depths the there was higher energy at the diurnal and semi-diurnal periods, the energy was aperiodic. A higher energy band at the 6 – 10 day period was present at all three depths (circled in red), being strongest at 74 m (this will be compared later with to the wind stress wavelets).

In the SC3 alongshore and cross-shore wavelet spectra with depth (Figure III-22) the same results were obtained as in SC2. The energy occurred in the near surface and near bottom with very little in the middle of the water column. At all three depths in SC3 (Figures III-23, 24, & 25) there was more dominant diurnal energy in the alongshore flow

and semi-diurnal current in the cross-shore flow. Between April 12 – 21, the April event, there was strong 2-3 day period with energy present all three depths in the alongshore flow and strongest at 74 m (Figure III-24).

In order to investigate the April event in greater detail, a two month (March 15 – May 15, 2007) period was analyzed. The rotary wavelet power spectra for all depths (Figure III-26) were computed in order to take a closer look at the diurnal-inertial band. Clockwise energy was dominant over the counterclockwise energy. In the clockwise power spectrum there was higher energy in the upper layer and bottom layer, however the energy peaks between the two layers were not contiguous. At ~65 m there was little energy present. Looking at the rotary wavelet spectra at the same three depths as before, (Figure III-27, 28, & 29) there were intermittent periods of enhanced near-inertial/diurnal and semi-diurnal energy in the clockwise and very little seen in the counterclockwise spectra. Between April 1 and April 6 there was a very strong event at 34 m that was dominated by the clockwise energy but still fairly strong in the counterclockwise (circled in red in Figure III-27). Nearly rectilinear motion only appeared at the near surface (34 m) depth. The April event was not present near surface. The clockwise wavelet spectra had high energy at 2 days decreasing to 1 day (near inertial/diurnal period) and the counterclockwise wavelet spectra had very weak energy during the event time frame. At mid-depth (74 m), the clockwise and counterclockwise energy appeared equal during the April, making it rectilinear (Figure III-28). The near bottom (110 m) counterclockwise energy was dominant over the clockwise energy, meaning the currents were slowly rotating in the counterclockwise direction (Figure III-29). At all three depths intermittent modes of higher energy at the near-inertial/diurnal and semi-diurnal periods (only in the clockwise rotary wavelet) were observed. The strongest intermittent modes of near inertial/diurnal and semi-diurnal energy were observed at the near bottom depth. Over all, the clockwise energy was dominant at all depths. The near surface alongshore and cross-shore velocity components (Figure III-30) show the same high energy mode at the near-inertial/diurnal period that was coincident with the rotary wavelet spectra. The April event was very weak in the near surface in the alongshore flow. However, at the

mid-depth (Figure III-31) the April event was strongest in the alongshore component, and it also appears at near bottom (Figure III-32).

Wavelet power spectra were computed from the U and V wind stress components for all three buoy stations: TB, SMB, and SCB. The time frame for the wind stress spectra ran from July 10, 2006 through May 10, 2007 (the data gap at SCB buoy, prompted this ending time). Little diurnal and semidiurnal energy was observed at the three wind stations. Most of the energy was observed at periods greater than two days. Higher energy observed at the 6 – 10 day period (Figure's III- 33, 34, & 35) beginning September 6, 2007 through the beginning of October 2007, was coincident with the higher energy observed in the currents for the same time period. This higher energy could be due to a storm passing through the area. Based upon these observations, the April event does not appear to be induced by the wind stress from any of the three buoy locations.

H. WIND STRESS FORCING

1. Wind Stress and Curl

Many large and small scale ocean circulations are dependent upon the interaction of the atmosphere and ocean. Winds in the bight were generally weak, but were highly variable in comparison to winds north of Point Conception. The wind stress values (the same values which were used in the wavelet analysis) for all three NDBC buoy stations: TB, SCB, and SMB were computed using the procedure suggested by Large and Pond (1981) using a neutral drag coefficient. The wind stress time-series for all three stations (Figure III-36) were computed to compare the sheltering effects at each station. SCB and SMB have relatively weak wind stress values. Tanner Banks is on the western edge of the bight and the open ocean. The TB buoy was not affected by the sheltering that occurred within the bight so naturally the wind stress was going to be much larger at this location.

The curl of the wind stress was calculated from these three NDBC buoy stations. The wind stress and the alongshore currents were smoothed to 10 days using a 4^{th} Order Butterworth filter. The curl of the wind stress was compared to the alongshore currents

(Figure III-37). This was done to investigate the possible forcing of the current reversals. No visual correlation was found and a cross-correlation computation confirmed this conclusion (figure not shown).

2. Wind Forced Slab Model

The location of Eel Point mooring, 32˚ N latitude, is considered a critical latitude for diurnal-inertial resonance. At 30˚ latitude, the inertial frequency is equal to the frequency of the diurnal tide (Craig, 1989). In order to investigate if inertial oscillations are prevalent at this location, a simple slab model following Pollard and Millard (1970) was created. The simple slab model uses the wind stress to predict if there are any inertial oscillations as result of the forcing.

The wind stress calculated from the SCB buoy was used to force the model of predicted inertial currents. The model uses a simple slab for input of the stress from the atmosphere. This model follows that discussed in Paduan et al. (1989), using the formulation from Pollard and Millard (1970). In order to compute the inertial currents, $Q = u + i\upsilon$ (Q is the inertial current) is driven by the surface wind stress $\rho\Upsilon = \tau^x + i\tau^y$. The wind stress is taken up uniformly over a slab of depth *h* (which is treated as a constant):

$$\frac{dQ}{dt} + \Omega Q = \frac{\Upsilon}{h},$$

(equation 1 in Paduan et al. 1989) where Ω = r + *if* and *r* is the Raleigh frictional decay included with a an *e*-folding time of r^{-1} = 88 hours. The solution is:

$$Q = Q_0 e^{-\Omega t} + \int_0^t \frac{\Upsilon}{h} e^{-\Omega(t-t')} dt,$$

(equation 2 in Paduan et al. 1989) where Q_0 is the initial current and equal to zero for this study.

This model uses complex demodulation at the near inertial frequency. It removes low frequency and tidal motions which are not expected to be correlated with the local wind.

For this analysis, unsmoothed wind stress values computed from SCB buoy were used in order for the model to predict oscillatory current responses. The mixing layer was set to h = 34 m for comparison with the complex demodulated near surface currents at depths 34 m. There were periods of inertial motion output with this model. The currents at 34 m do not reflect any inertial frequency oscillations predicted by the model (Figures not shown). However, there was a strong near inertial/diurnal mode of energy in the 2-month wavelet spectra in the along and cross-shore flow. This higher energy was only observed at the near surface. The demodulated currents at 34 m showed a peak in the current speed at the same time of the observed higher energy in the spectra (around April 4, 2007), the inertial oscillation was not predicted by the model using the SCB buoy wind stress. The model was run using the demodulated currents at 38 m and there was no peak in the current speed observed, so the energy was only associated with near surface currents < 38 m. It was possible there may have been other inertial frequency oscillations in the near surface which did not penetrate to 34 m. These could not be determined with this data set, since the top bin was so deep and wind stress used in the model was not localized to the Eel Point mooring.

Table 1. ADCP statistical results from the observed (unsmoothed/unrotated) data. U and V component values of the mean, maximum, minimum and standard deviation.

Depth	Mean U (cm/s)	Max U (cm/s)	Min U (cm/s)	Mean V (cm/s)	Max V (cm/s	Min V (cm/s)	Standard Deviation U (cm/s)	Standard Deviation V (cm/s)
26 m	-2.2	25.4	-31.5	2.4	38.6	-23.1	5.9	6.8
30 m	-2.0	25.6	-28.9	2.8	38.6	-21.7	5.9	7.0
34 m	-1.8	27.9	-31.3	2.9	42.0	-21.0	6.0	7.1
38 m	-1.7	28.0	-30.2	3.0	41.8	-22.2	6.0	7.3
42 m	-1.5	28.5	-29.8	3.0	44.0	-22.8	6.2	7.5
46 m	-1.4	28.4	-32.3	3.0	44.2	-24.9	6.3	7.7
50 m	-1.2	29.4	-33.2	3.0	40.6	-29.1	6.4	7.9
54 m	-1.1	31.5	-33.7	3.0	40.1	-27.6	6.5	8.0
58 m	-1.1	28.6	-33.0	3.1	39.0	-27.3	6.6	8.0
62 m	-1.1	24.7	-35.2	3.1	41.1	-25.6	6.7	8.1
66 m	-1.2	27.3	-38.7	3.2	40.3	-25.7	6.7	8.2
70 m	-1.2	27.4	-41.5	3.3	45.1	-26.4	6.8	8.2
74 m	-1.2	25.7	-43.1	3.4	43.6	-29.6	6.9	8.3
78 m	-1.3	29.6	-38.8	3.6	45.1	-28.8	7.0	8.4
82 m	-1.5	32.1	-43.0	3.7	40.3	-29.3	7.1	8.5
86 m	-1.7	33.4	-42.7	3.8	42.7	-27.3	7.3	8.7
90 m	-1.8	32.8	-42.2	3.9	41.9	-26.7	7.5	8.7
94 m	-2.1	36.4	-42.7	4.1	42.4	-32.1	7.7	8.8
98 m	-2.2	30.4	-42.0	4.3	46.2	-45.6	7.9	8.8
102 m	-2.3	28.9	-42.4	4.4	44.1	-27.0	8.0	8.9
106 m	-2.3	32.2	-42.2	4.5	44.8	-32.9	8.2	9.0
110 m	-2.4	31.3	41.5	4.4	45.4	-80.2	8.4	9.4
114 m	-2.4	37.4	-51.2	4.2	46.7	-46.5	8.6	9.5
118 m	-2.3	58.4	-61.1	3.9	45.4	-74.7	9.0	9.9

Table 2. Principal Axes.

Depth	Semi-Major Axis Direction T°	Semi-Major Axis Magnitude (cm/s)	Semi-Minor Axis Magnitude (cm/s)
26 m	328.2	7.3	5.4
30 m	329.4	7.5	5.3
34 m	330.1	7.6	5.3
38 m	331.8	7.8	5.4
42 m	332.8	7.9	5.6
46 m	333.3	8.1	5.8
50 m	334.0	8.3	5.9
54 m	334.4	8.4	6.1
58 m	333.6	8.5	6.1
62 m	332.5	8.6	6.1
66 m	331.5	8.7	6.1
70 m	330.4	8.9	6.0
74 m	329.4	9.1	6.0
78 m	327.8	9.2	5.9
82 m	326.7	9.4	5.9
86 m	325.6	9.7	6.0
90 m	324.7	9.8	6.1
94 m	323.6	9.9	6.2
98 m	322.5	10.0	6.4
102 m	321.6	10.1	6.5
106 m	321.5	10.3	6.6
110 m	323.1	10.6	7.0
114 m	322.9	10.7	7.2
118 m	322.7	11.1	7.6

Table 3. The 5 dominant tidal constituents computed from the vertically averaged currents. O1 and K1 are diurnal and N2, M2 and S2 are semi-diurnal tides.

Tidal Constituents	Period (hours)	Major Axis (cm/s)	Minor Axis (cm/s)	Greenwich Phase (deg)
O1	25.82	2.2	0.1	130.34
K1	23.93	4.0	-0.5	139.33
N2	12.66	0.8	-0.5	173.37
M2	12.42	4.1	-0.8	187.46
S2	12.00	1.4	-0.2	226.63

Table 4. The 5 dominant tidal constituents computed from the 50 m MicroCAT pressure data.

Tidal Constituents	Amplitude (cm)	Greenwich Phase (deg)
O1	21.7	218.65
K1	34.2	207.14
N2	11.9	163.30
M2	48.8	170.41
S2	19.8	142.10

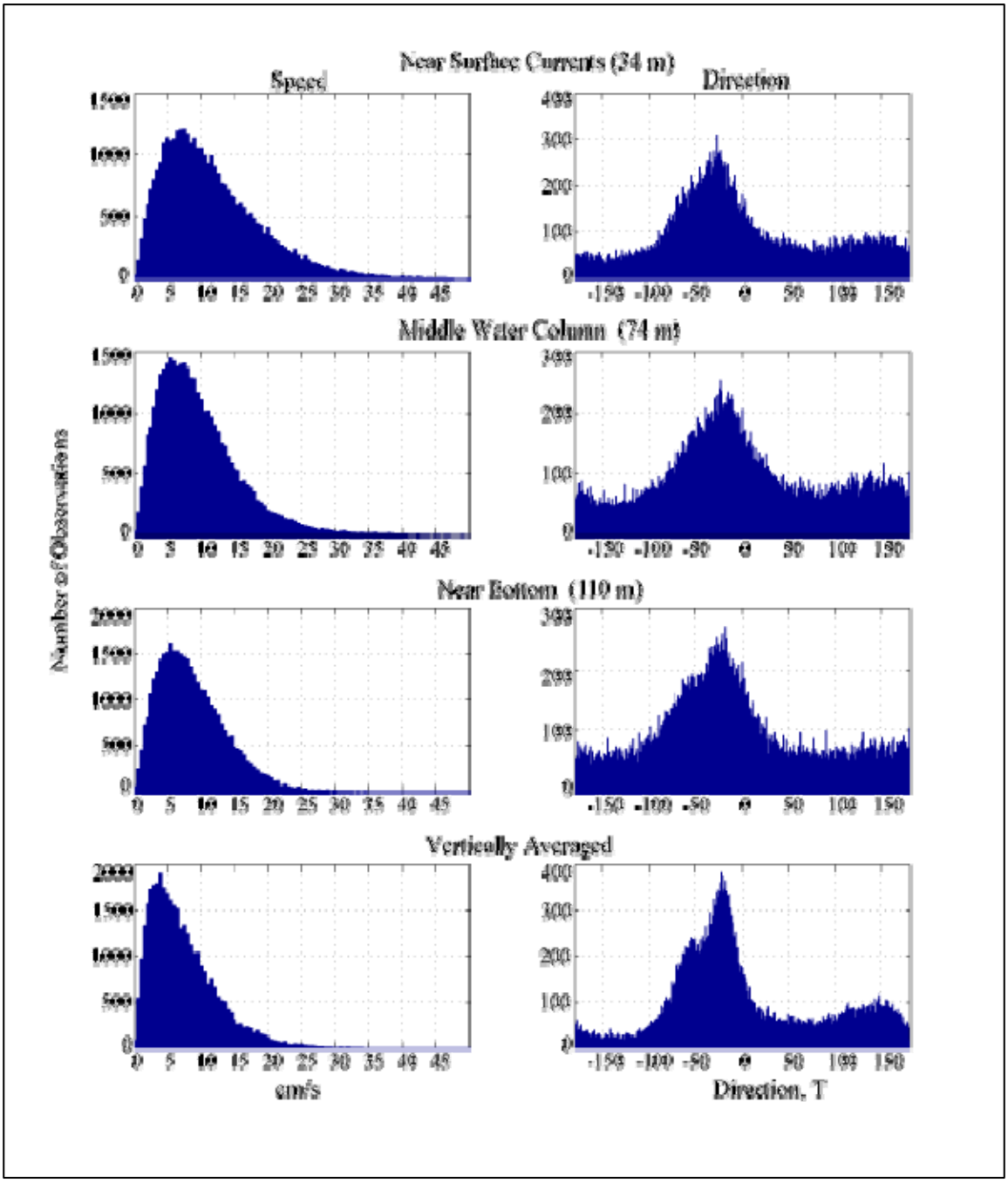

Figure III-1. Histogram of speed (left) and direction (right) for ADCP currents, at near surface (34 m), mid-water (74 m), near bottom (110 m), and vertically averaged.

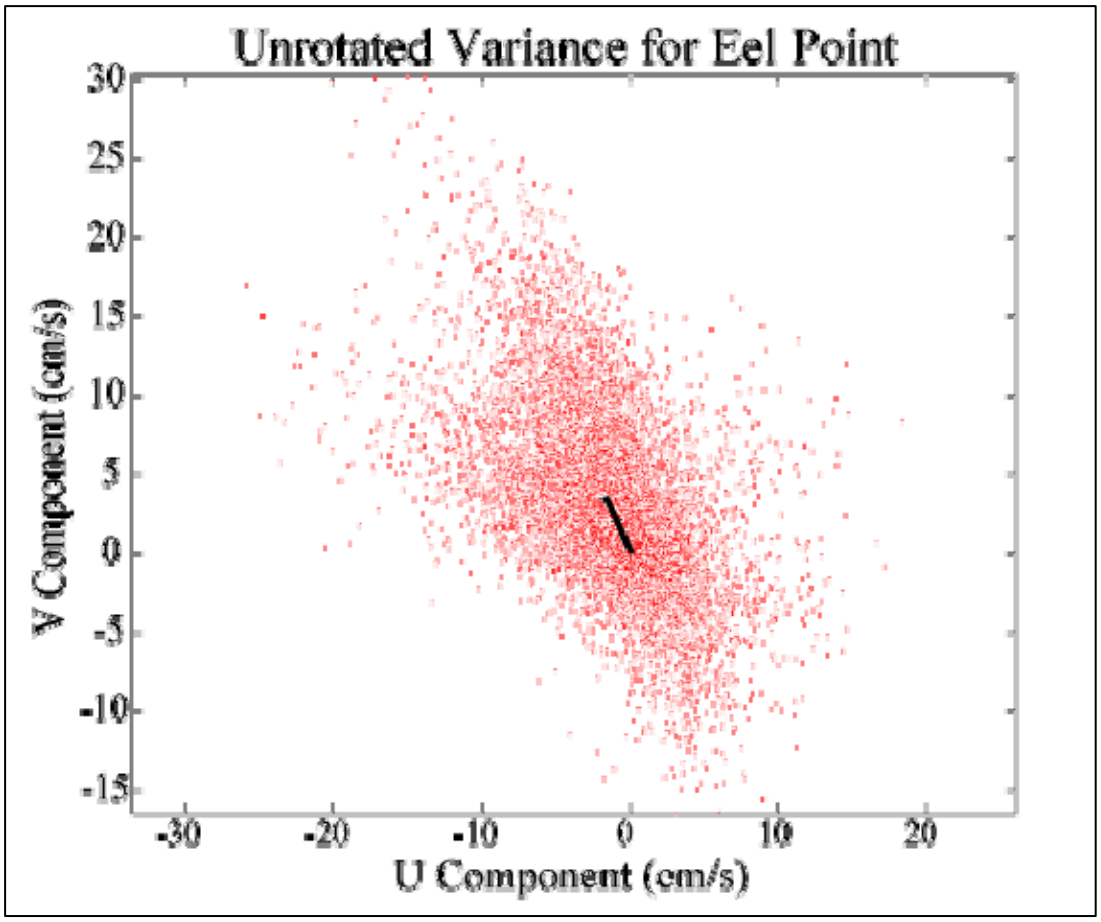

Figure III-2 Scatterplot generated from the Principal Axis Rotation. θ = 325˚ T.

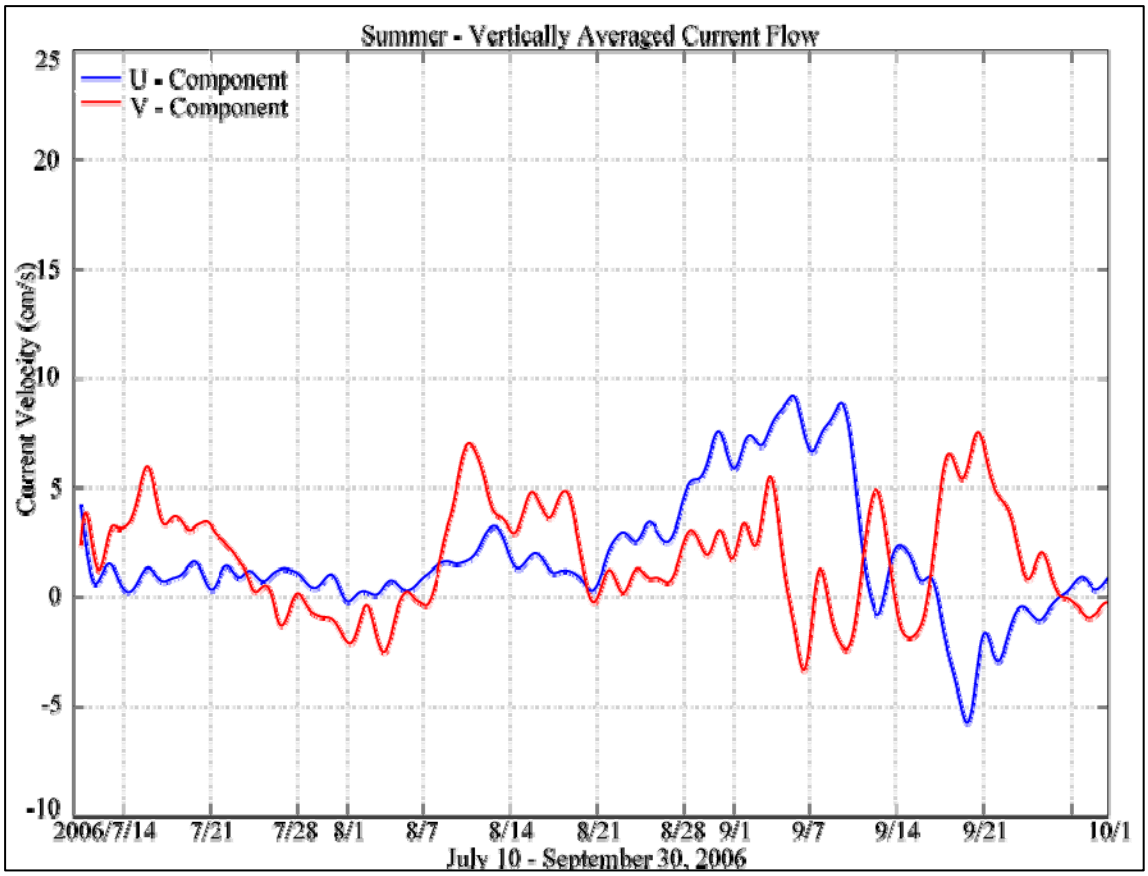

Figure III-3. Summer vertically averaged currents (data were rotated and vertically averaged over 24 bin depths between 26 m – 118 m).

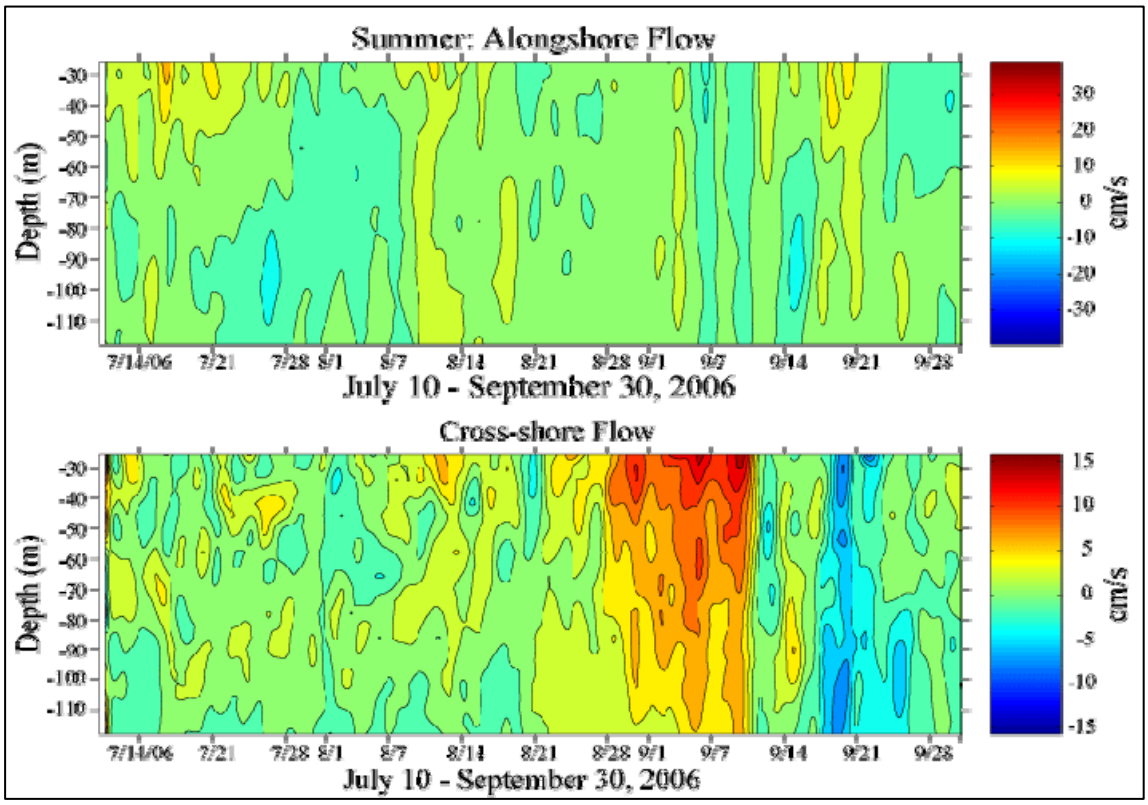

Figure III-4. Summer current velocities for the alongshore and cross–shore flow with depth. Alongshore flow was contoured from 35 to -35 at 5 cm/s intervals and the cross-shore flow was contoured from 15 to -15 at 2 cm/s intervals.

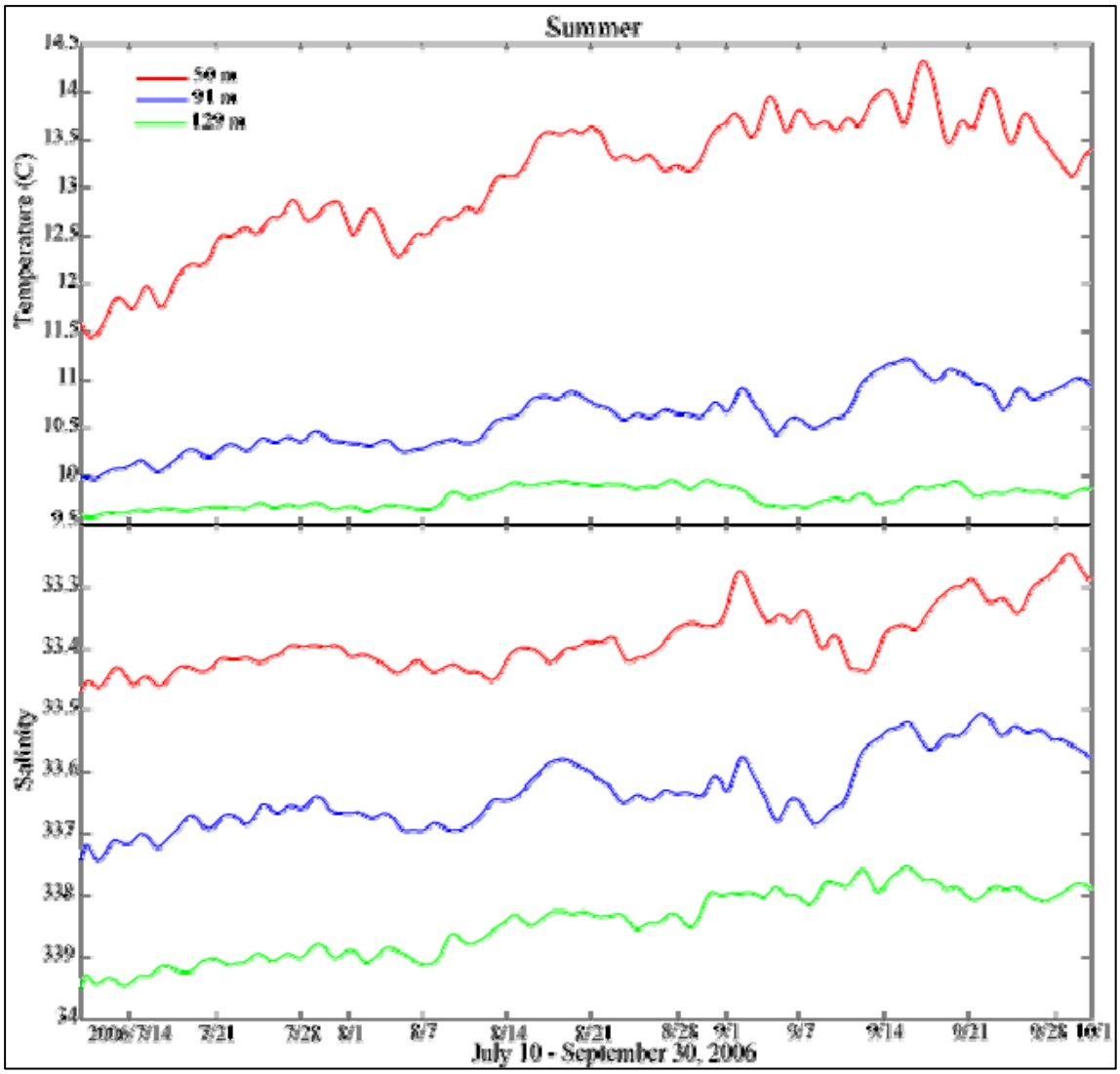

Figure III-5. Summer temperature and salinity measurements collected from the MicroCATs at depths: 50 m (red), 91m (blue), and 129 m (green).

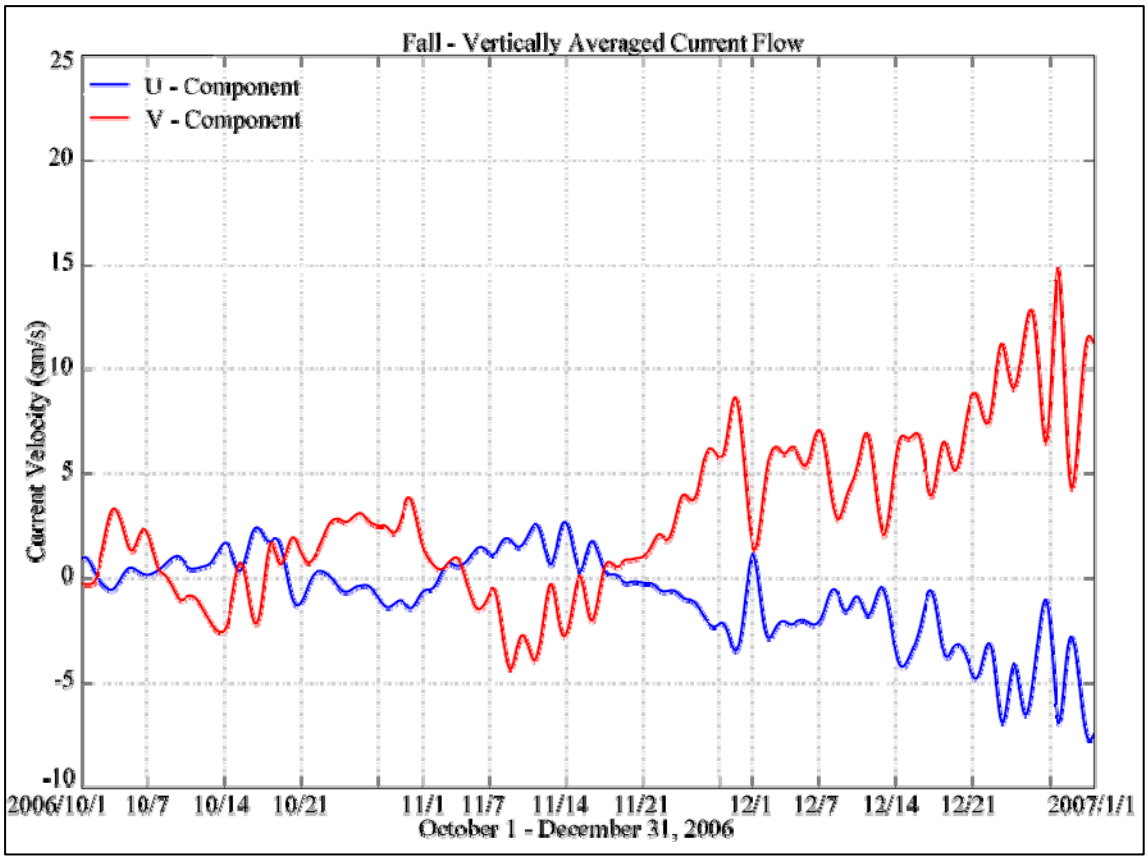

Figure III-6. Fall vertically averaged currents (data were rotated and vertically averaged over 24 bin depths between 26 m – 118 m).

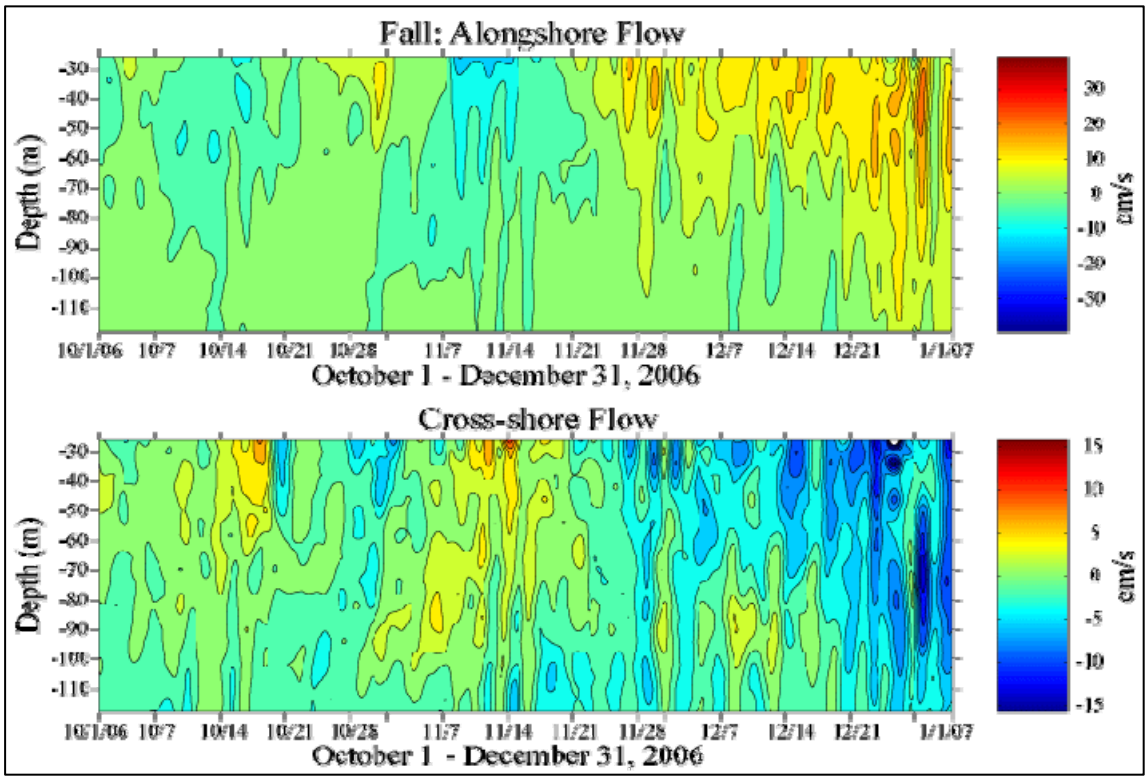

Figure III-7. Fall current velocities for the alongshore and cross–shore flow with depth. Alongshore flow was contoured from 35 to -35 at 5 cm/s intervals and the cross-shore flow was contoured from 15 to -15 at 2 cm/s intervals.

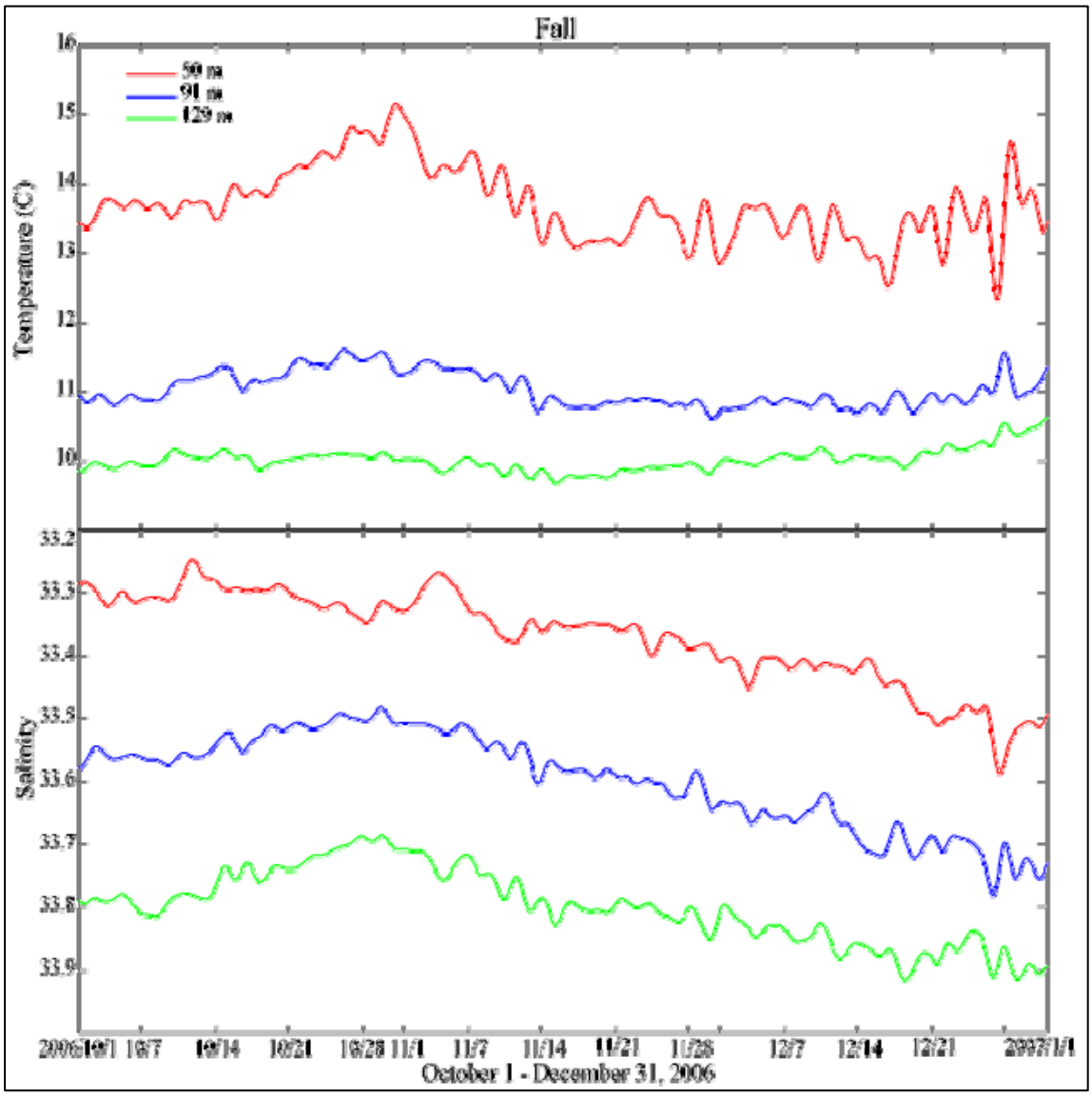

Figure III-8. Fall temperature and salinity measurements collected from the MicroCATs at depths: 50 m (red), 91m (blue), and 129 m (green).

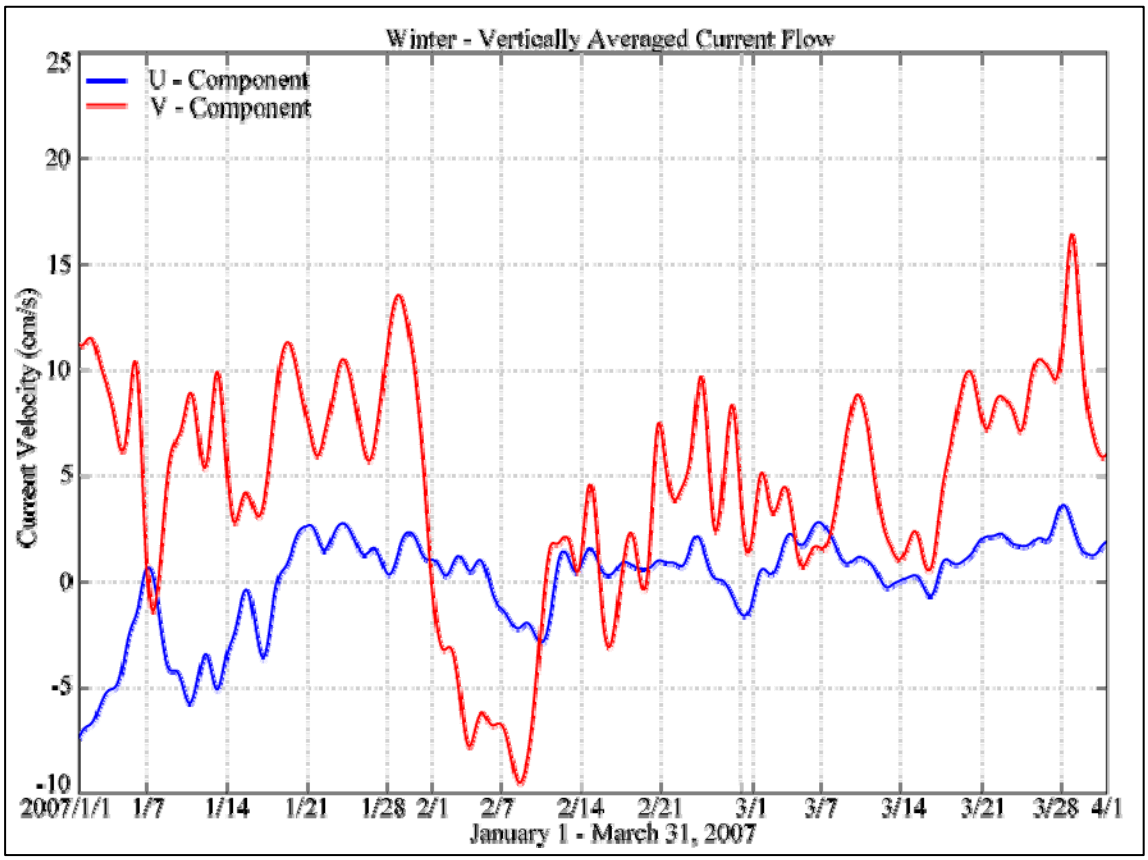

Figure III-9. Winter vertically averaged currents (data were rotated and vertically averaged over 24 bin depths between 26 m – 118 m).

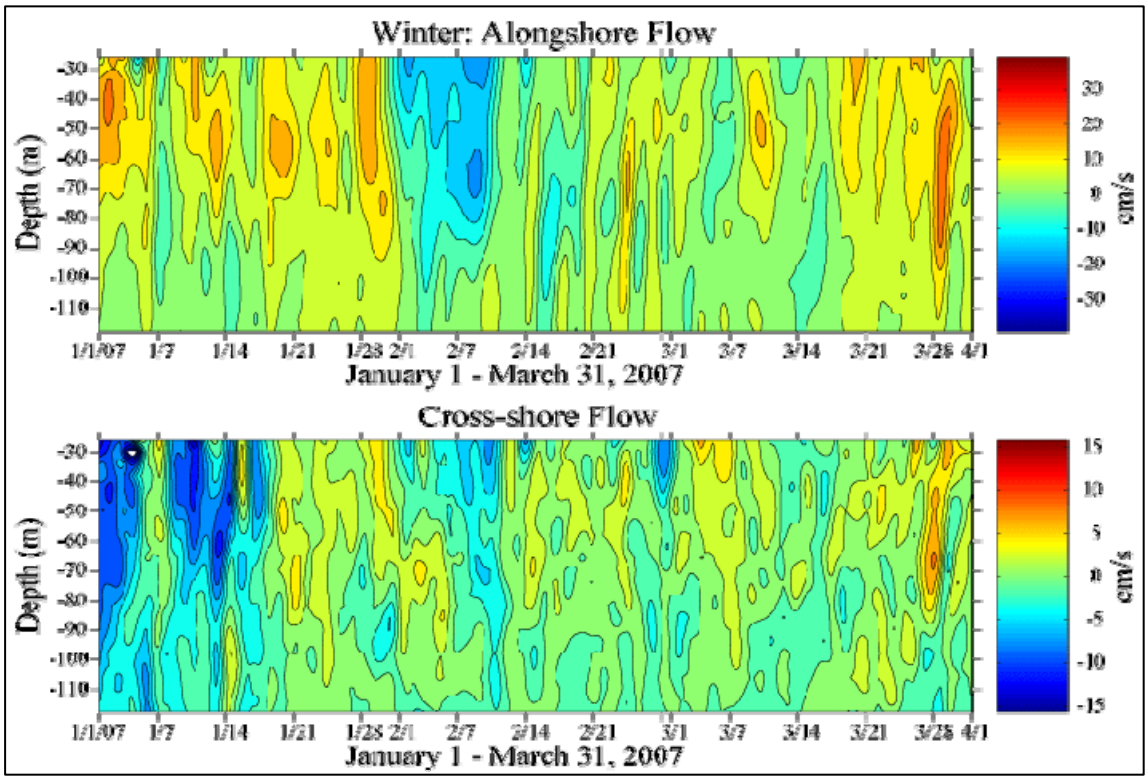

Figure III-10. Winter current velocities for the alongshore and cross–shore flow with depth. Alongshore flow was contoured from 35 to -35 at 5 cm/s intervals and the cross-shore flow was contoured from 15 to -15 at 2 cm/s intervals.

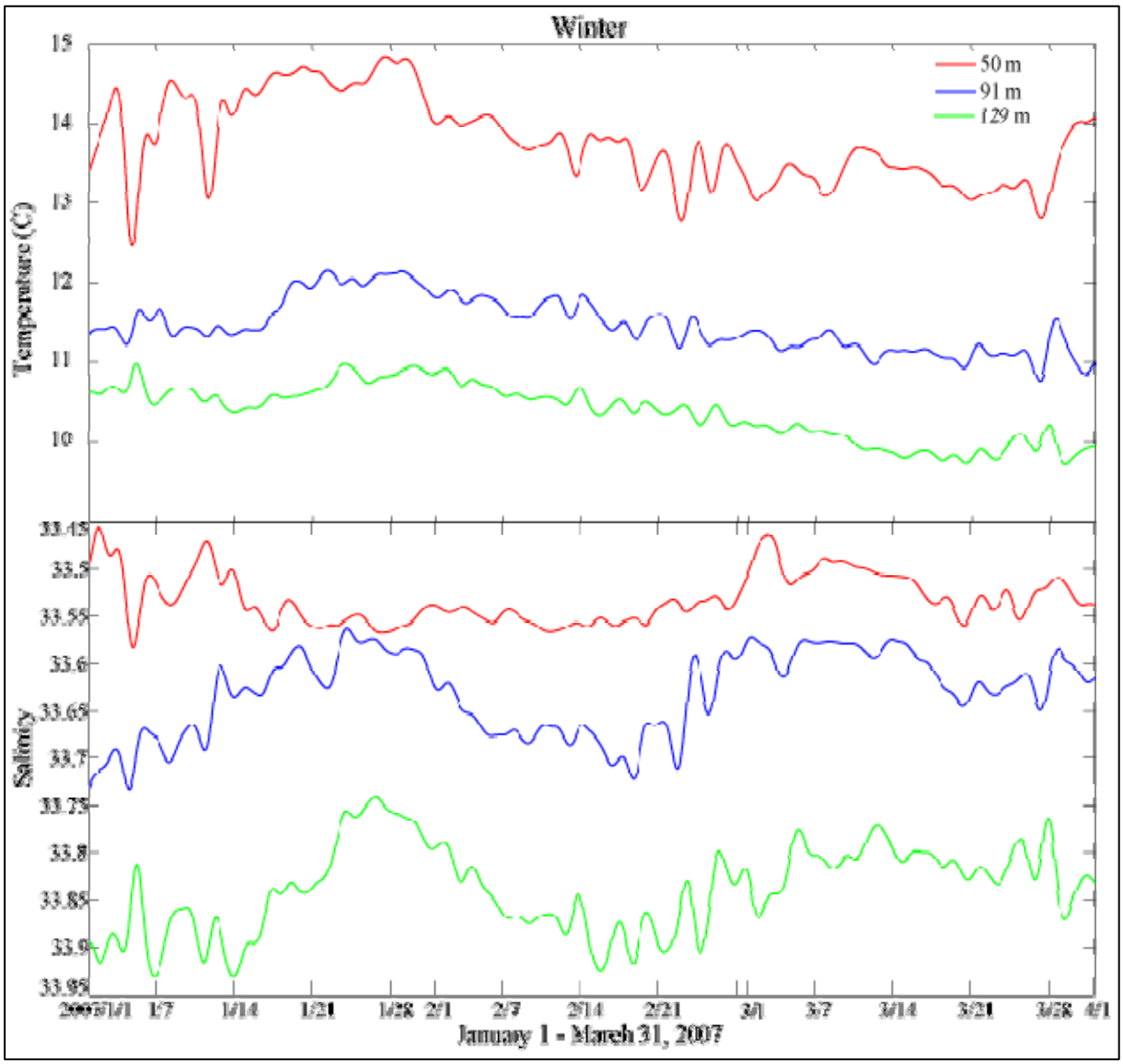

Figure III-11. Winter temperature and salinity measurements collected from the MicroCATs at depths: 50 m (red), 91m (blue), and 129 m (green).

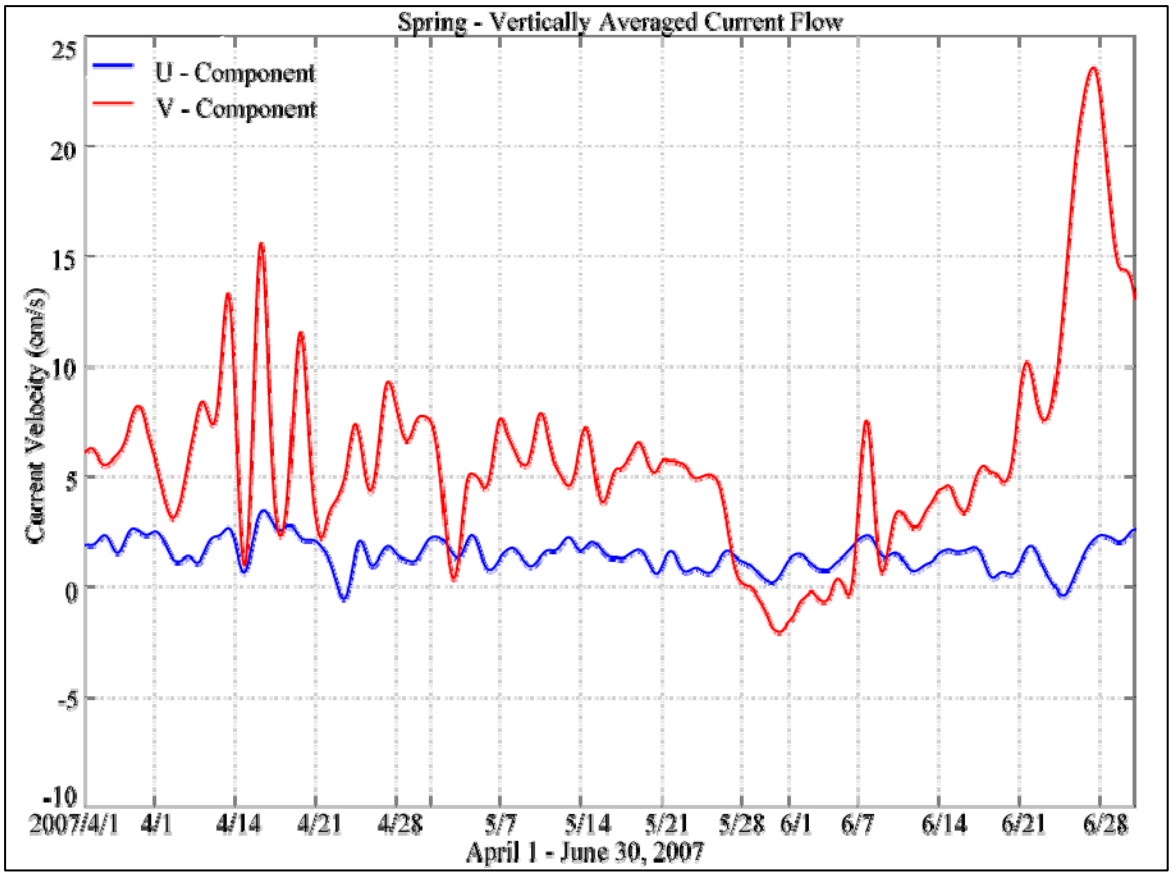

Figure III-12. Spring vertically averaged currents (data were rotated and vertically averaged over 24 bin depths between 26 m – 118 m).

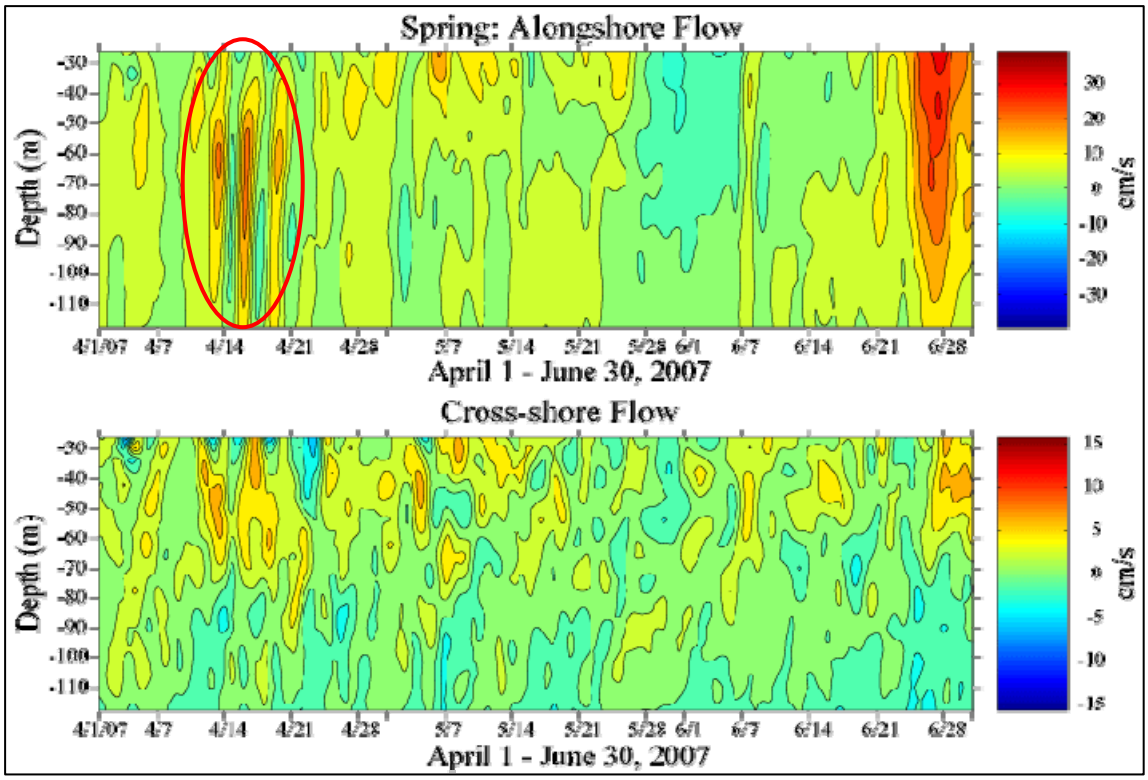

Figure III-13. Spring current velocities for the alongshore and cross–shore flow with depth. The oscillation is evident from the 12th to the 21st of April, which is referred to as the April event and circled in red above. (contour intervals are as previously mentioned).

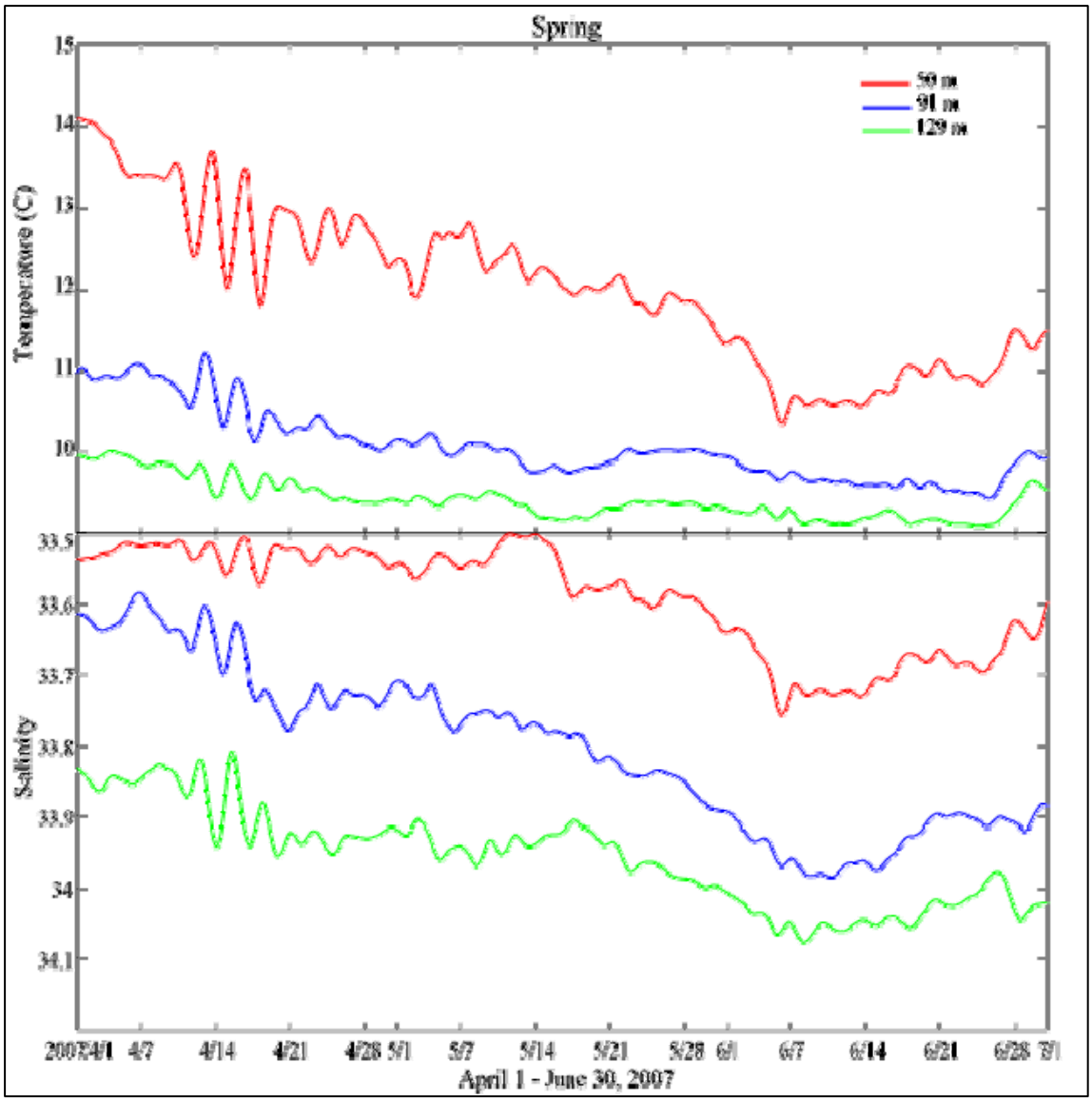

Figure III-14. Spring temperature and salinity measurements collected from the MicroCATs at depths: 50 m (red), 91m (blue), and 129 m (green).

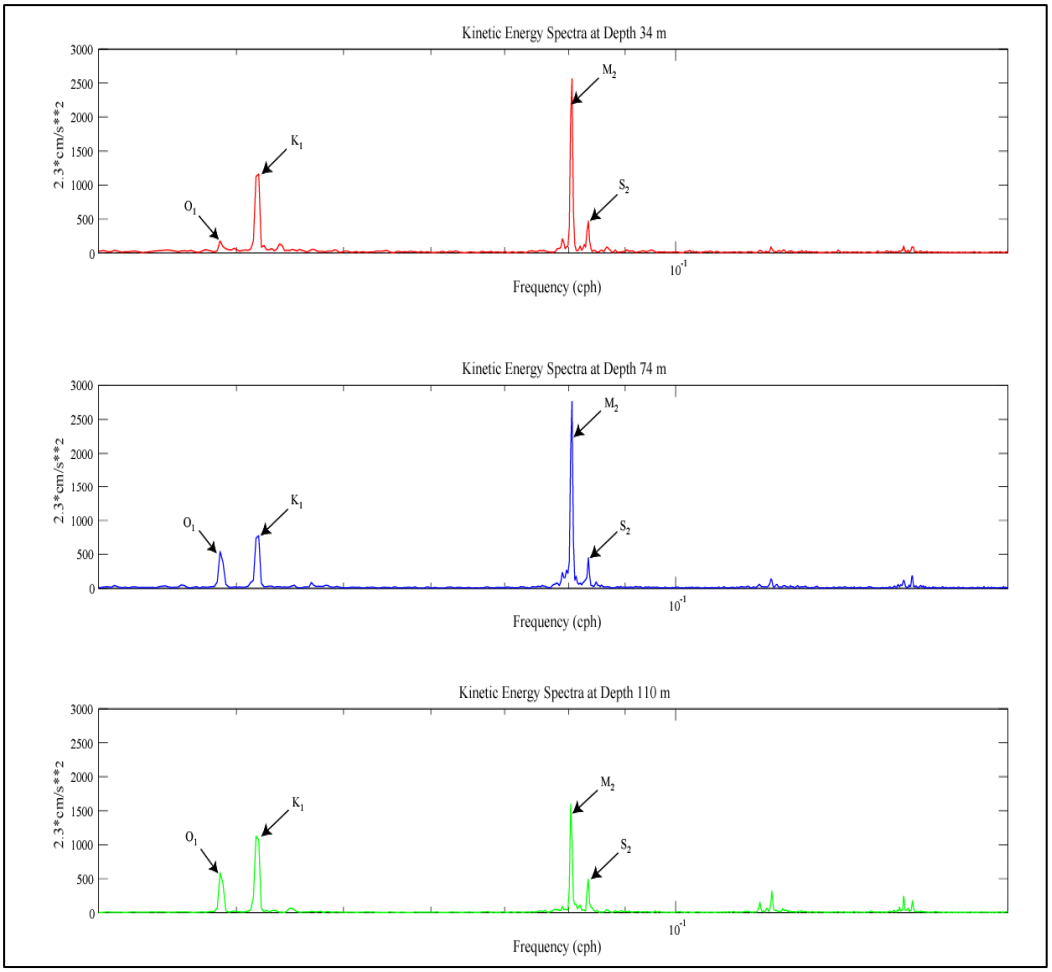

Figure III-15. Variance Preserving Kinetic Energy Spectra for near-surface (34 m), middle water column (74 m), and near-bottom (110 m). The spectra were dominated by energy in the semi-diurnal (M2 peak) and the diurnal (K1) tidal frequencies.

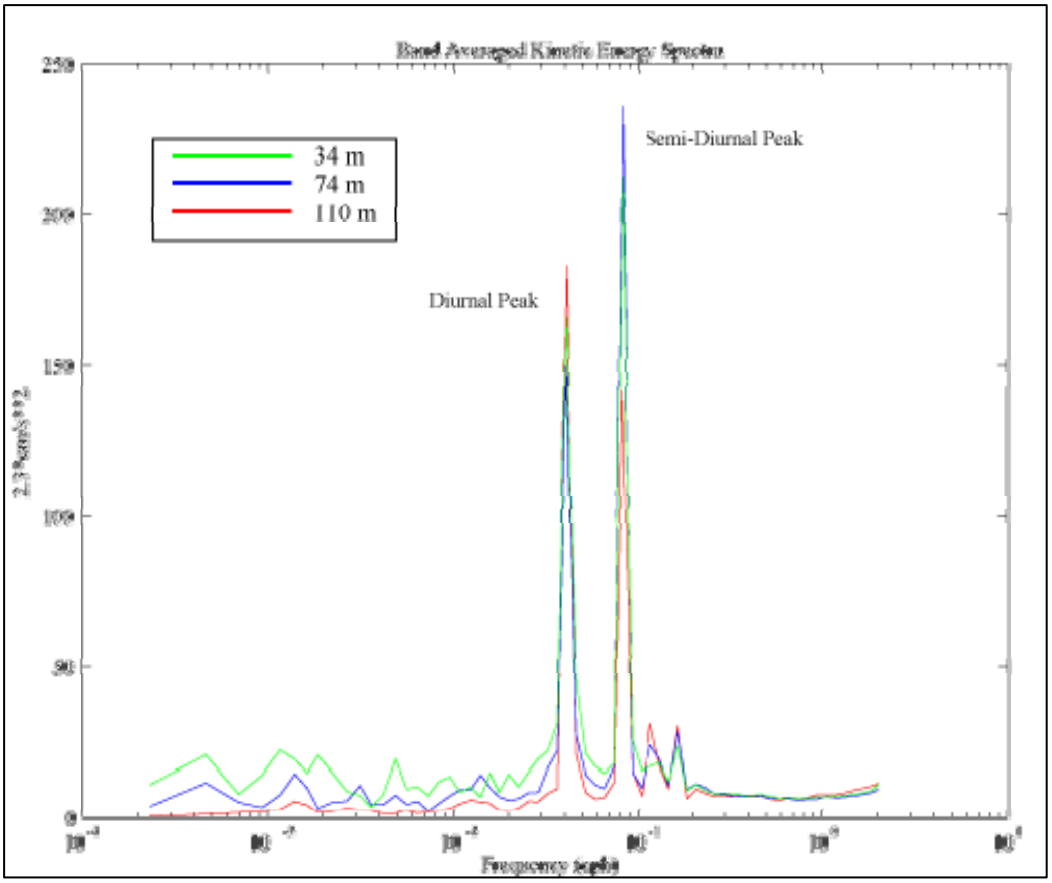

Figure III-16. Band averaged KE spectra, showing that dominant energy is in the semi-diurnal and diurnal frequencies.

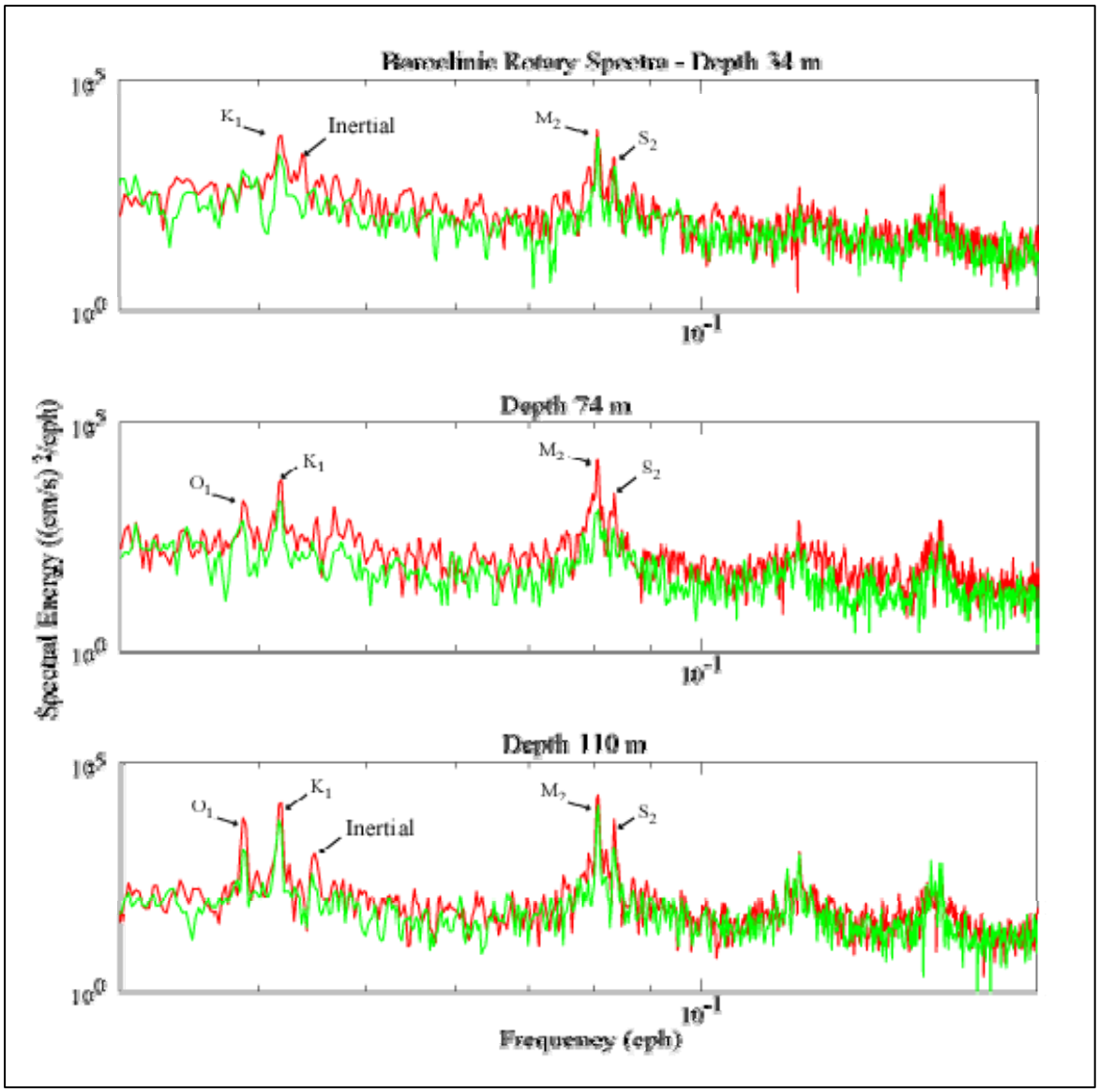

Figure III-17. Rotary Spectra for near-surface (34 m), mid-water (74 m) and near bottom (110 m). Red (green) is clockwise (counterclockwise).

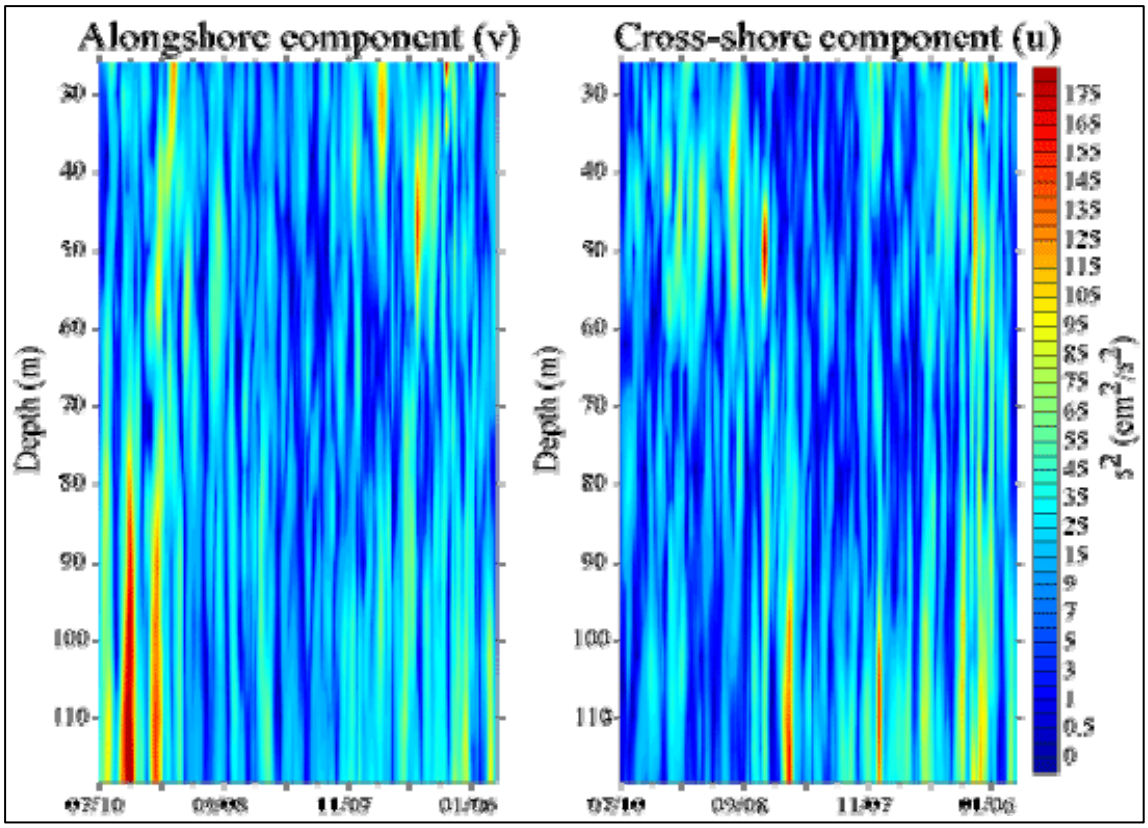

Figure III-18. SC2 wavelet spectra of the near-inertial/diurnal band with depth for the alongshore (v) and cross-shore (u) components. (Contour intervals are non-linear)

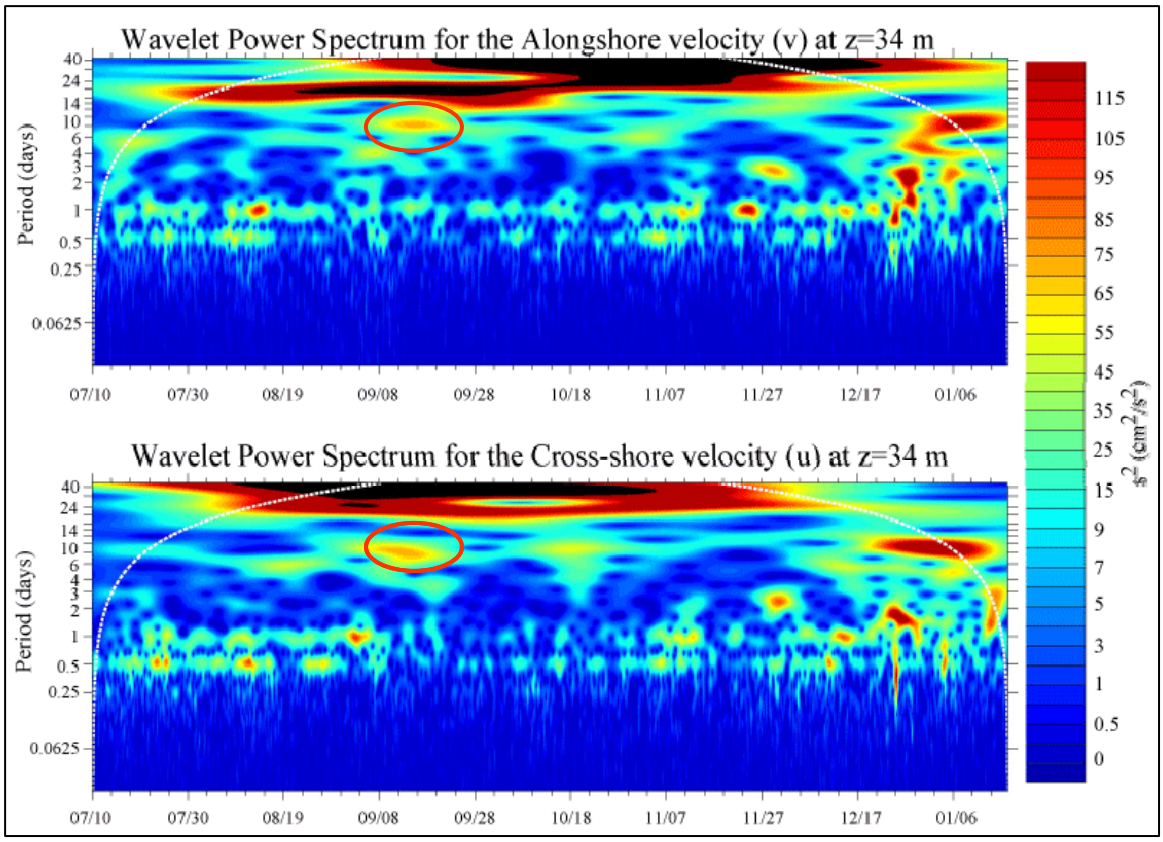

Figure III- 19 SC2 wavelet power spectra from July 10, 2006 – January 18, 2007, depth 34 m. Dashed white line is the COI. Higher modes of energy at the 6-10 day period, circled in red. (Contour intervals are non-linear)

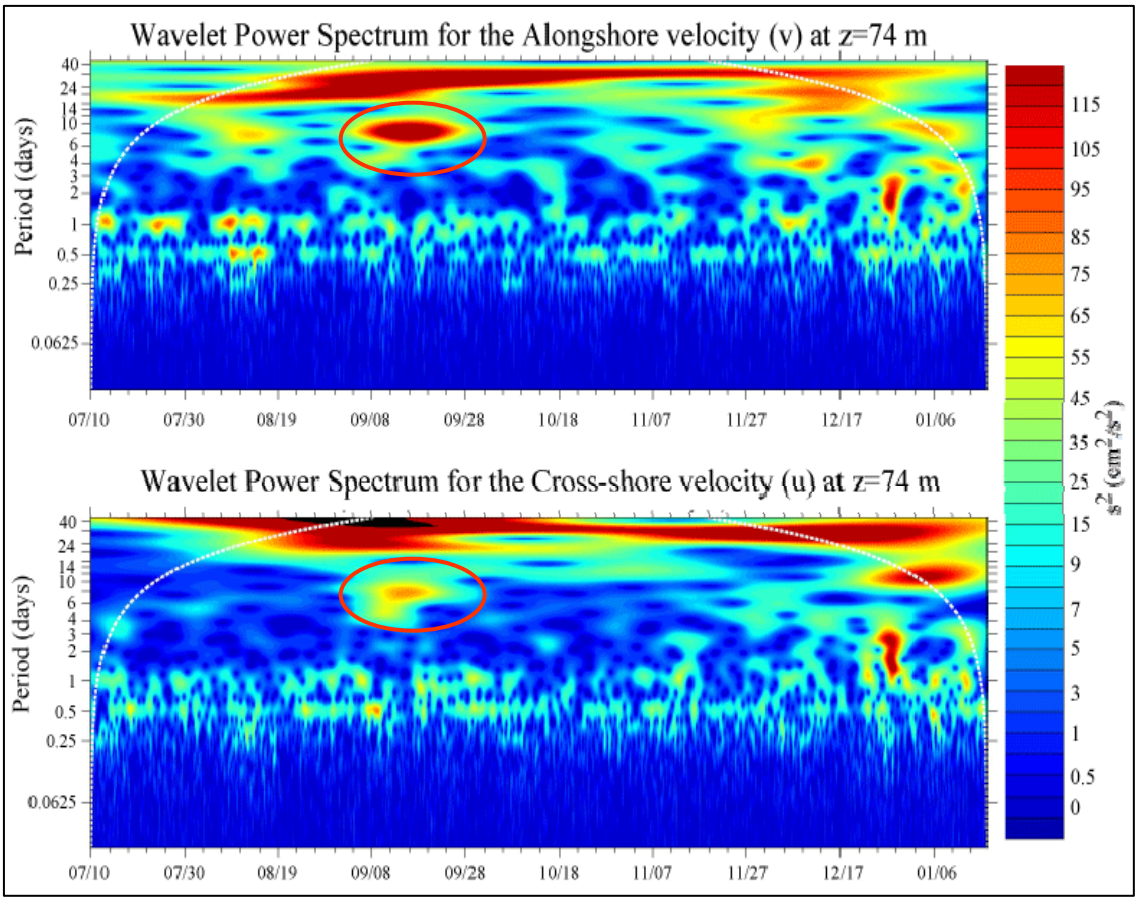

Figure III-20. SC2 wavelet power spectra from July 10, 2006 – January 18, 2007, depth 74 m. Higher modes of energy at the 6-10 day period are circled in red.

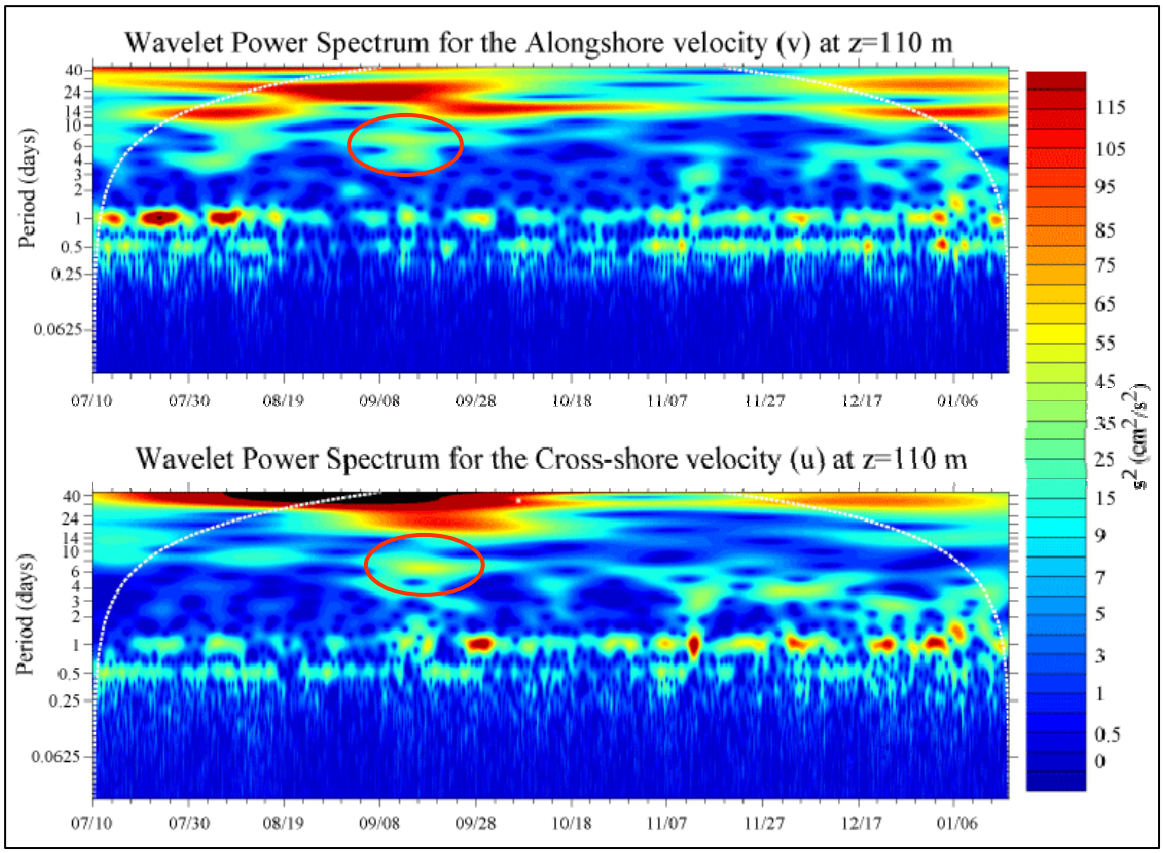

Figure III-21. SC2 wavelet power spectra from July 10, 2006 – January 18, 2007, depth 110 m. Higher modes of energy at the 6-10 day period are circled in red.

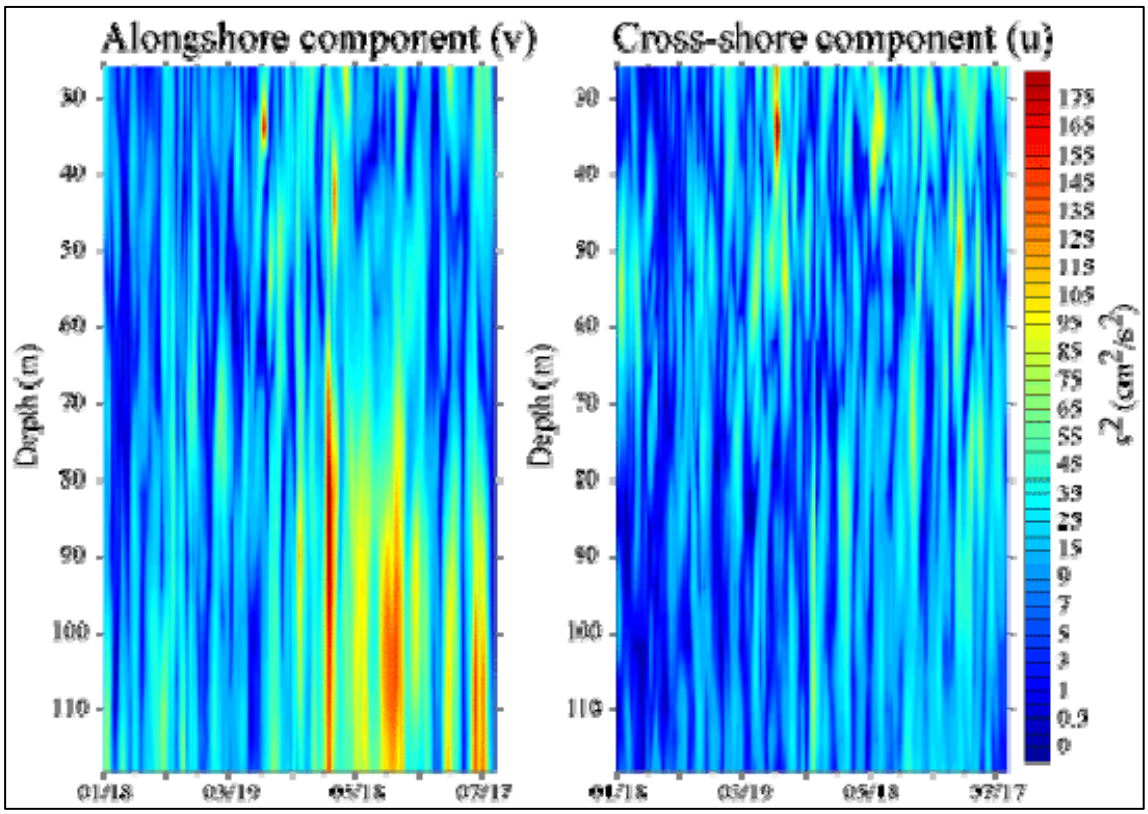

Figure III-22. SC3 wavelet spectra of the near-inertial/diurnal band with depth for the alongshore (v) and cross-shore (u) components.

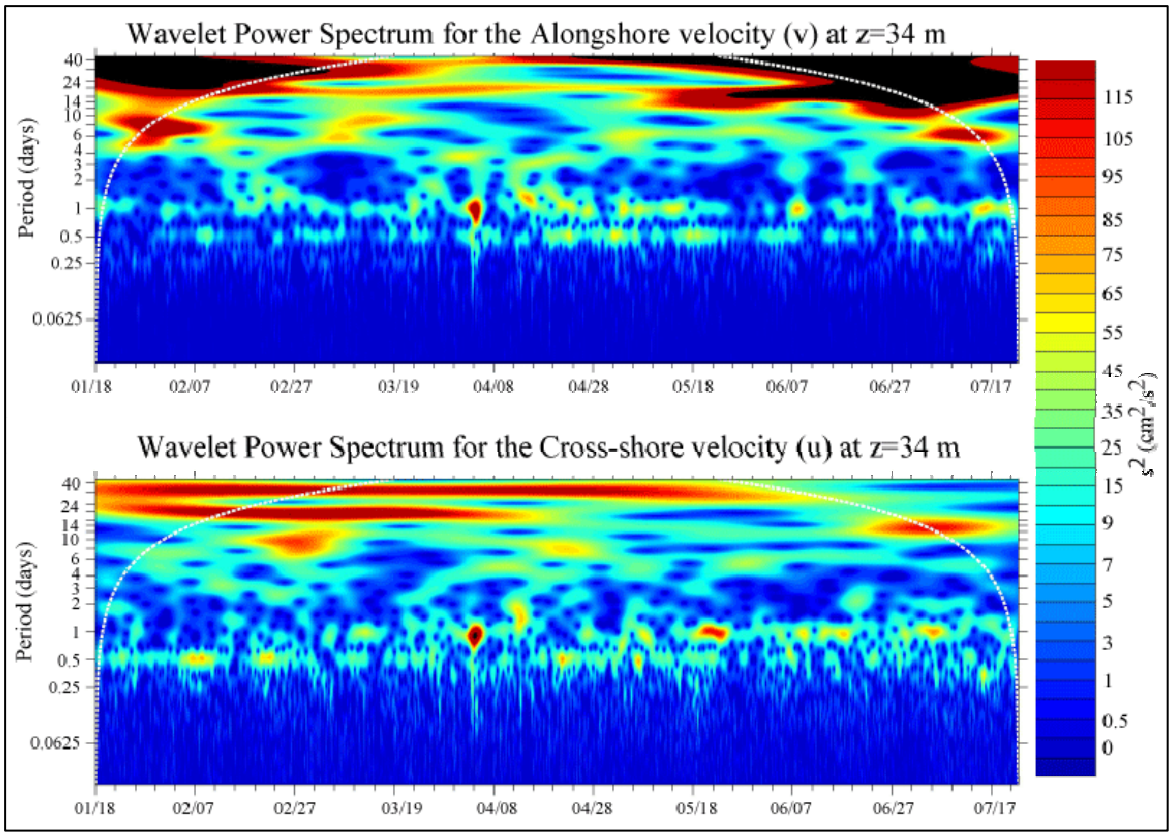

Figure III-23. SC3 wavelet power spectra from January 18, 2007, - July 23, 2007 depth 34 m. Dashed white line is the COI.

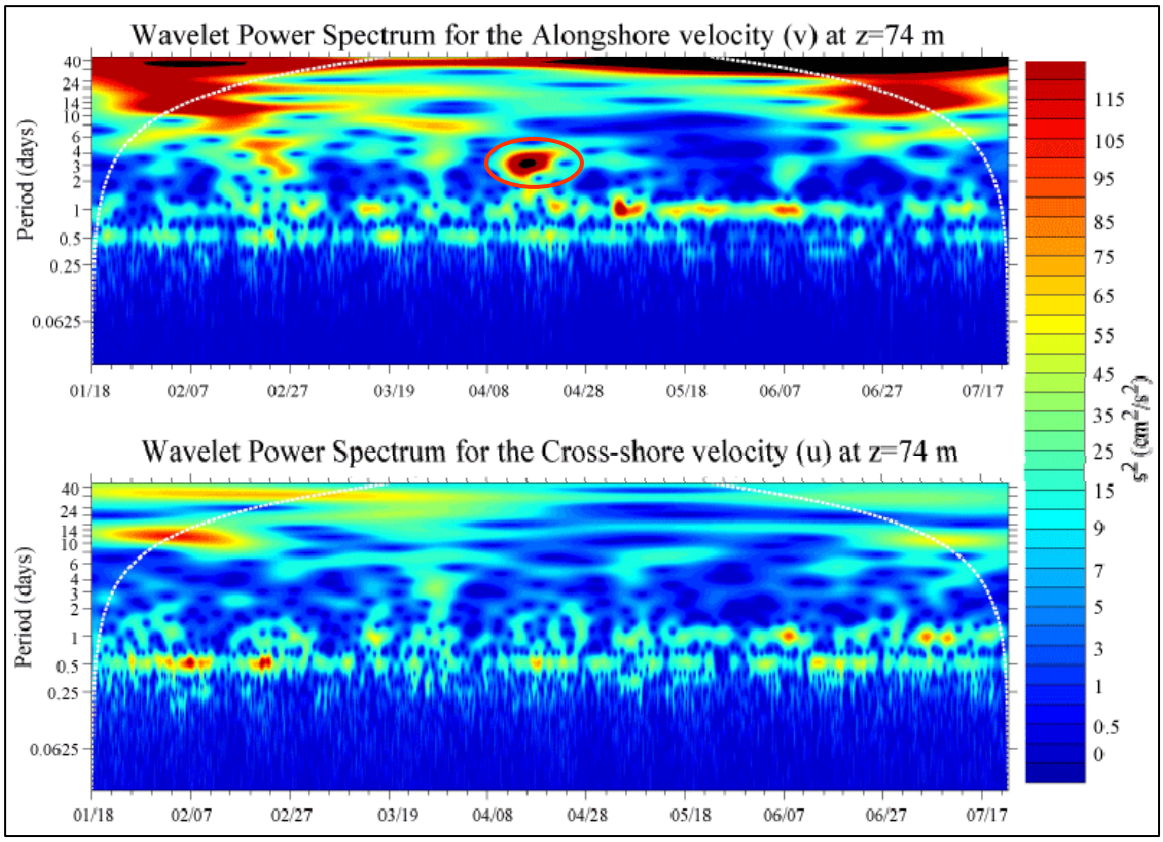

Figure III-24. SC3 wavelet power spectra from January 18, 2007, - July 23, 2007 depth 74 m. Higher mode of energy at the 2-3 day period are circled in red (April event).

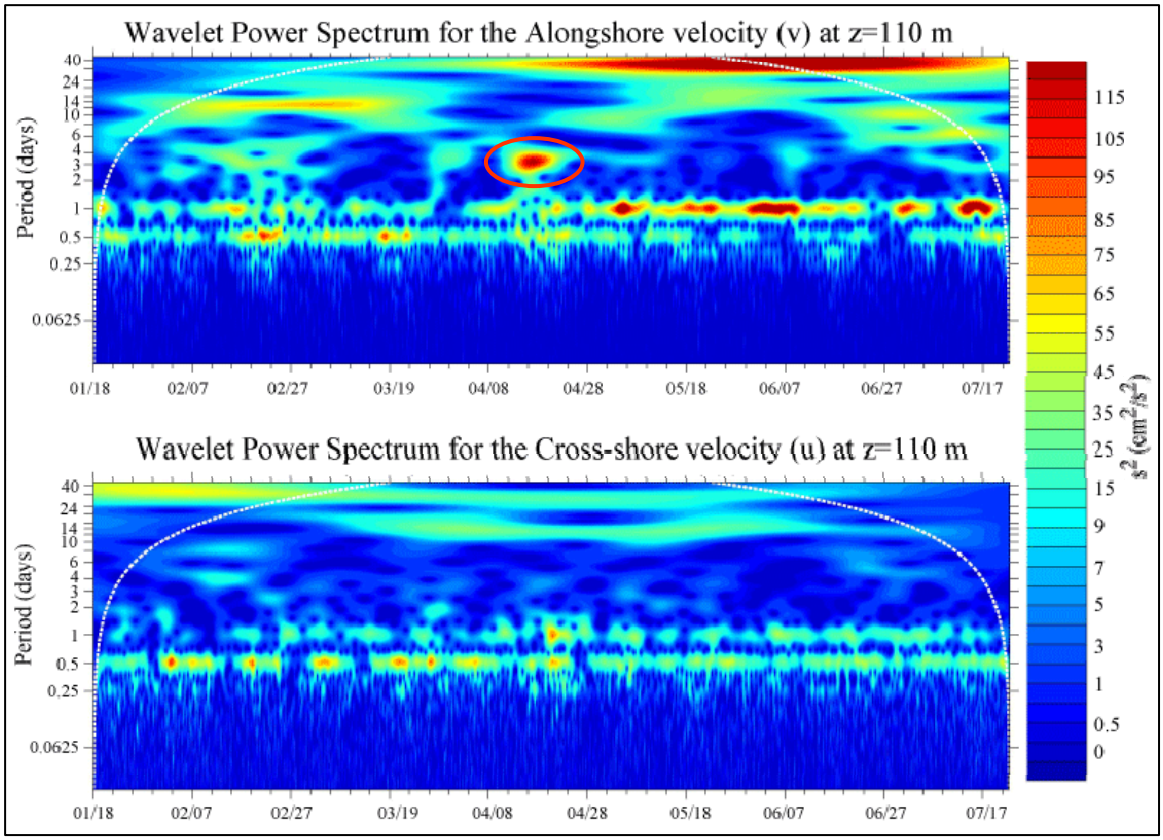

Figure III-25. SC3 wavelet power spectra from January 18, 2007, - July 23, 2007 depth 110 m. Higher mode of energy at the 2-3 day period are circled in red (April event).

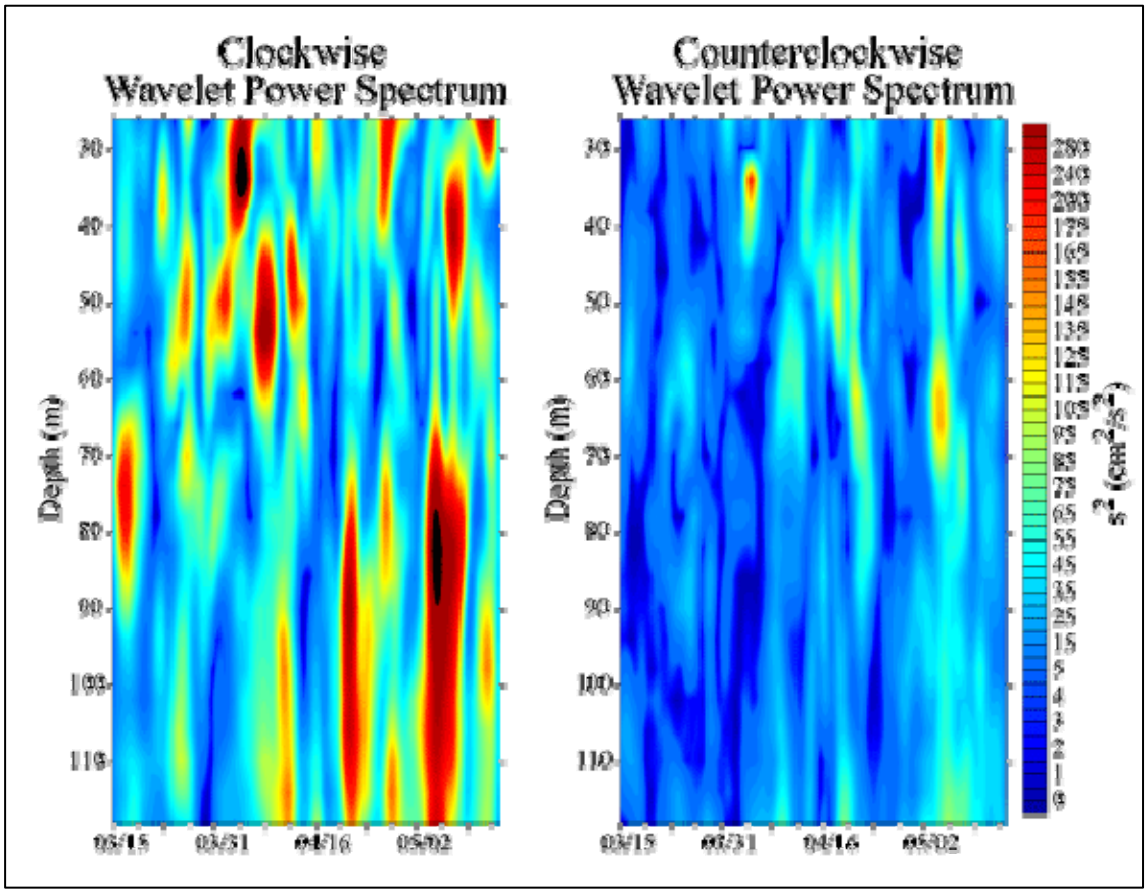

Figure III-26. Rotary wavelet power spectra for the period: March 15, - May 15, 2007, clockwise (counterclockwise) is on the right (left).

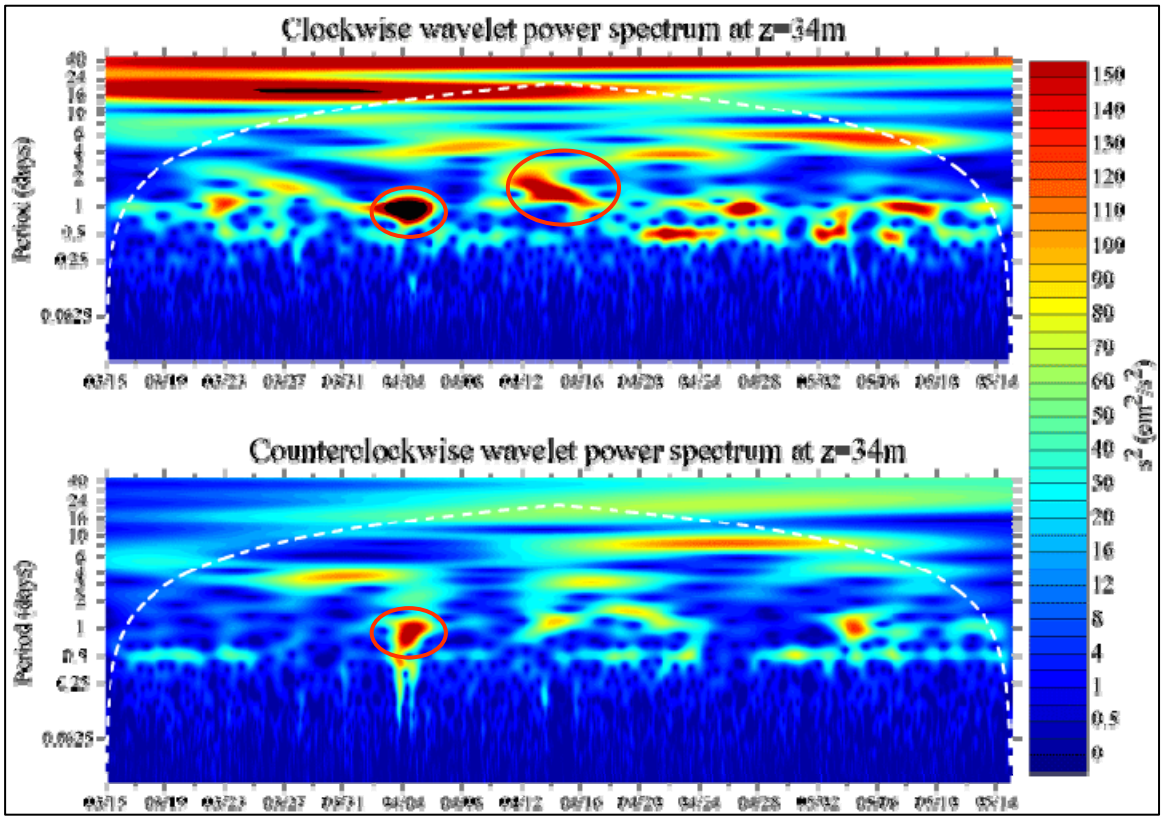

Figure III-27. Rotary wavelet power spectra for the period: March 15, - May 15, 2007, depth 34 m. Higher modes of energy at the near inertial/diurnal period and at the 2-1 day period are circled in red.

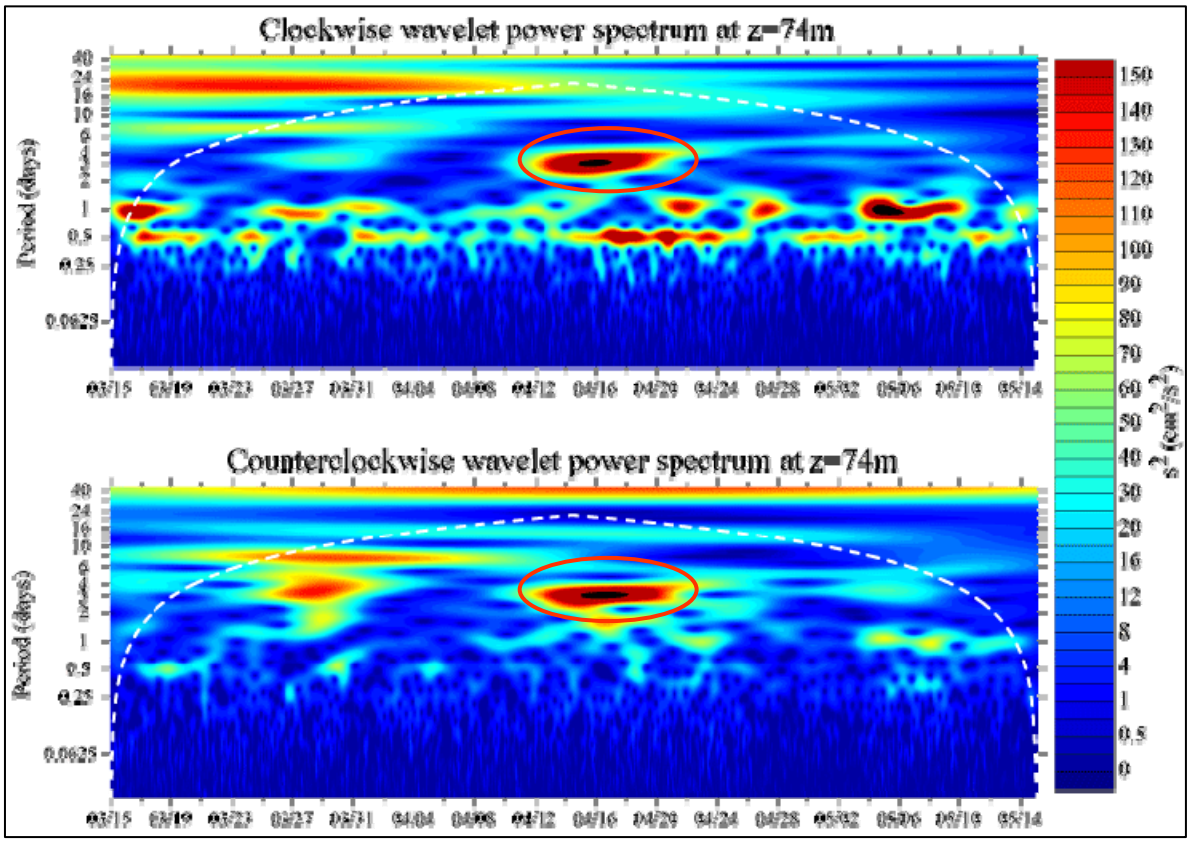

Figure III-28. Rotary wavelet power spectra for the period: March 15, - May 15, 2007, depth 74 m. Higher modes of energy at the 2-3 day period are circled in red (April event).

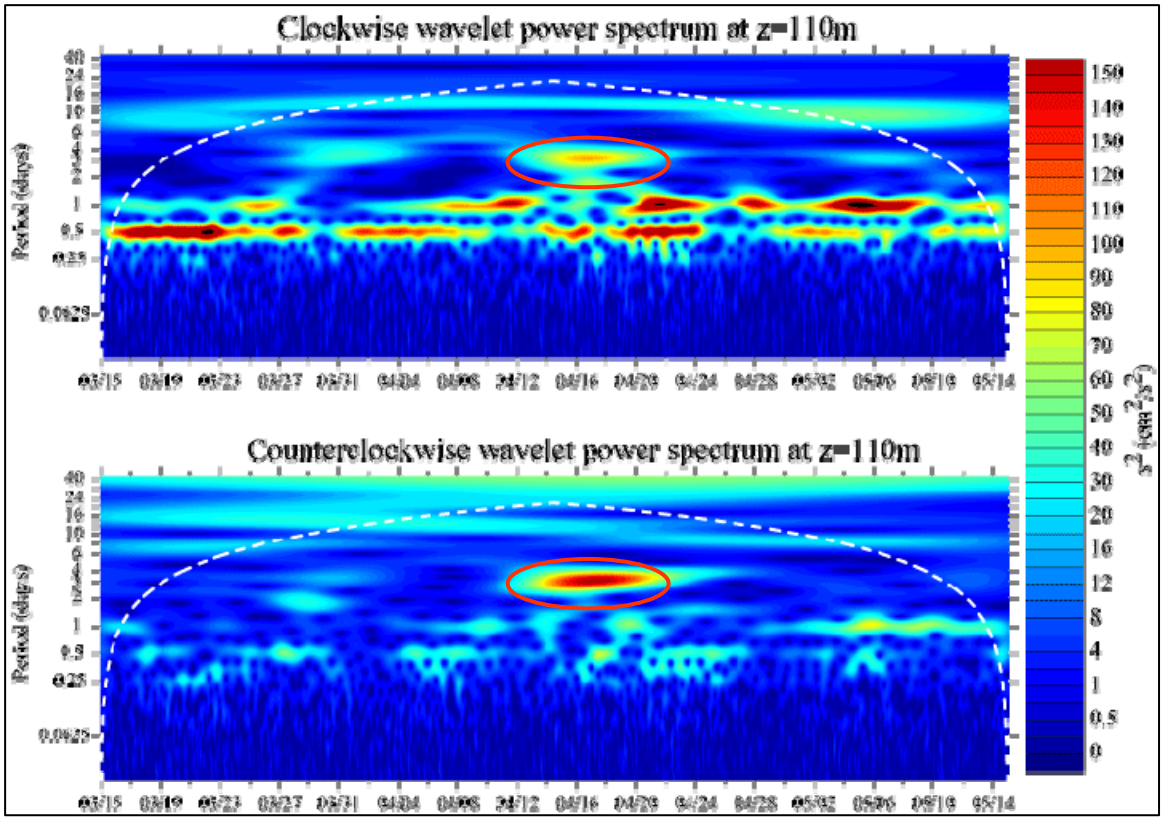

Figure III-29. Rotary wavelet power spectra for the period: March 15, - May 15, 2007, depth 110 m. Higher mode of energy at the 2-3 day period are circled in red (April event).

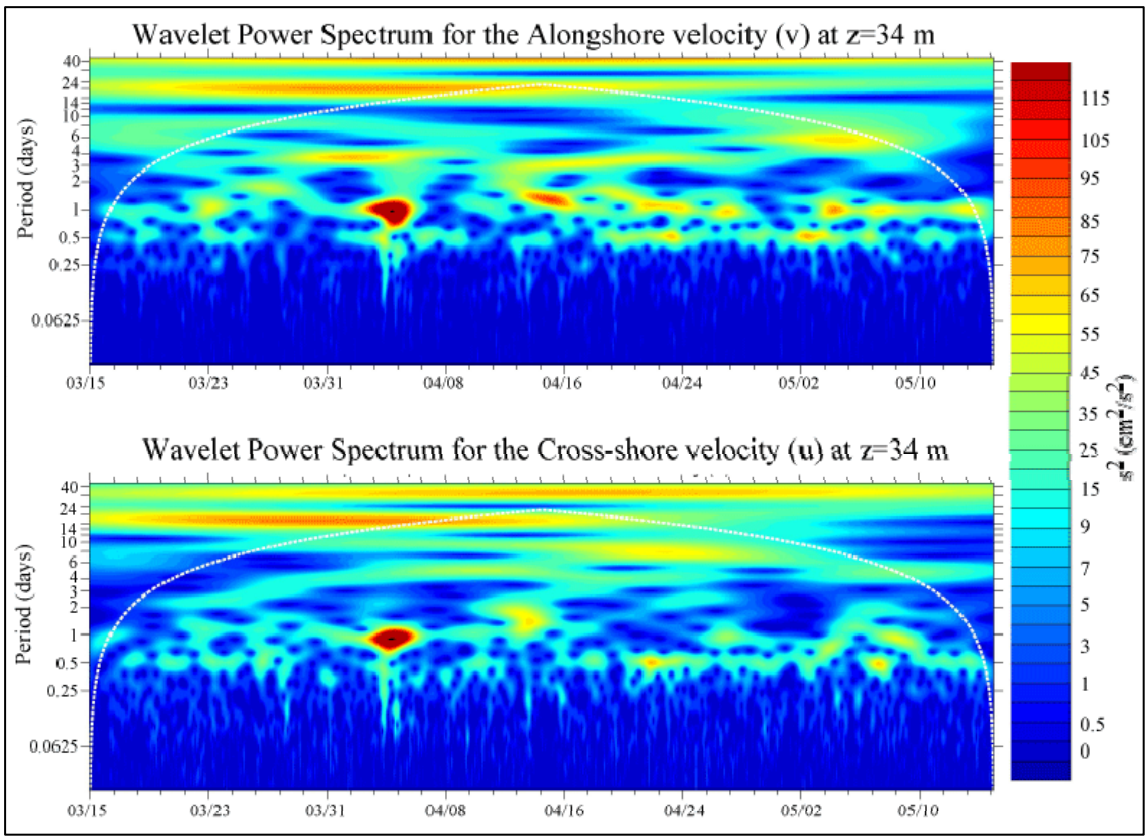

Figure III-30. Wavelet power spectra for the period: March 15 – May 15, 2007 at 34 m.

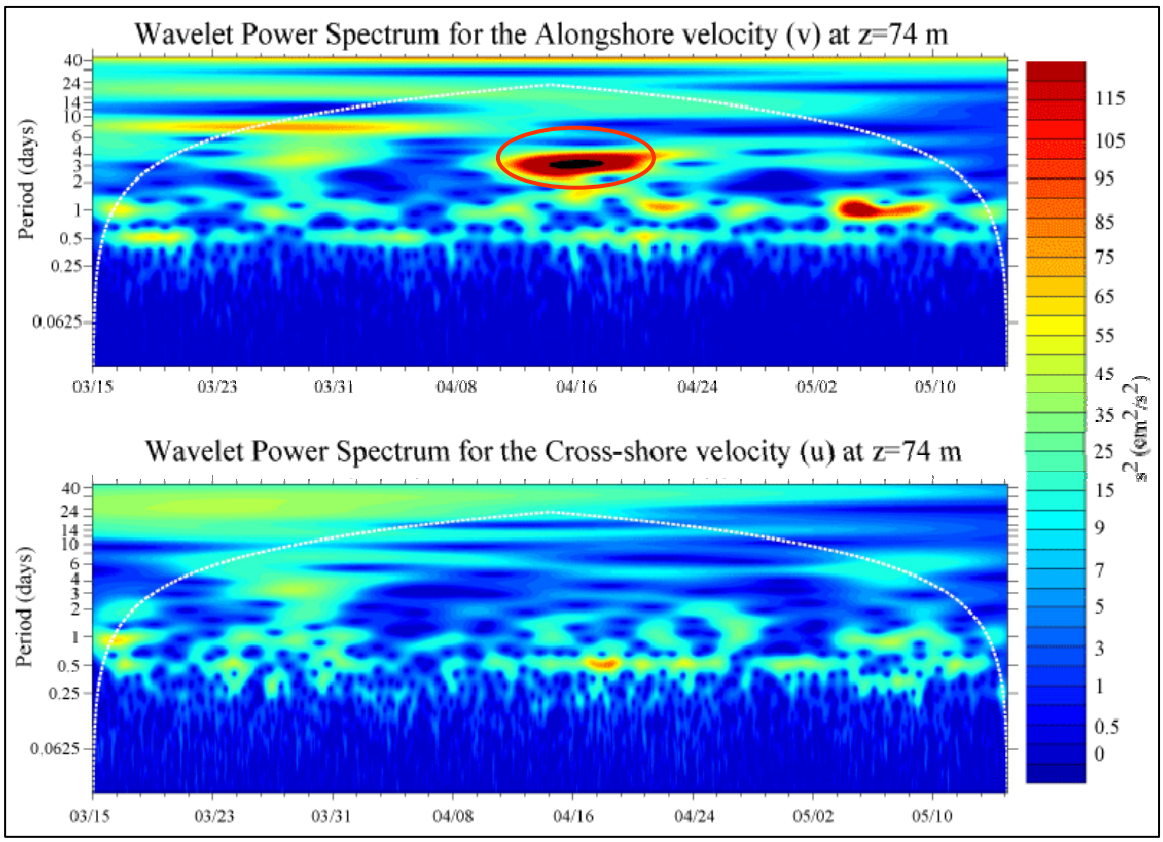

Figure III-31. Wavelet power spectra for the period: March 15 – May 15, 2007 at 74 m. Higher mode of energy at the 2-3 day period are circled in red (April event).

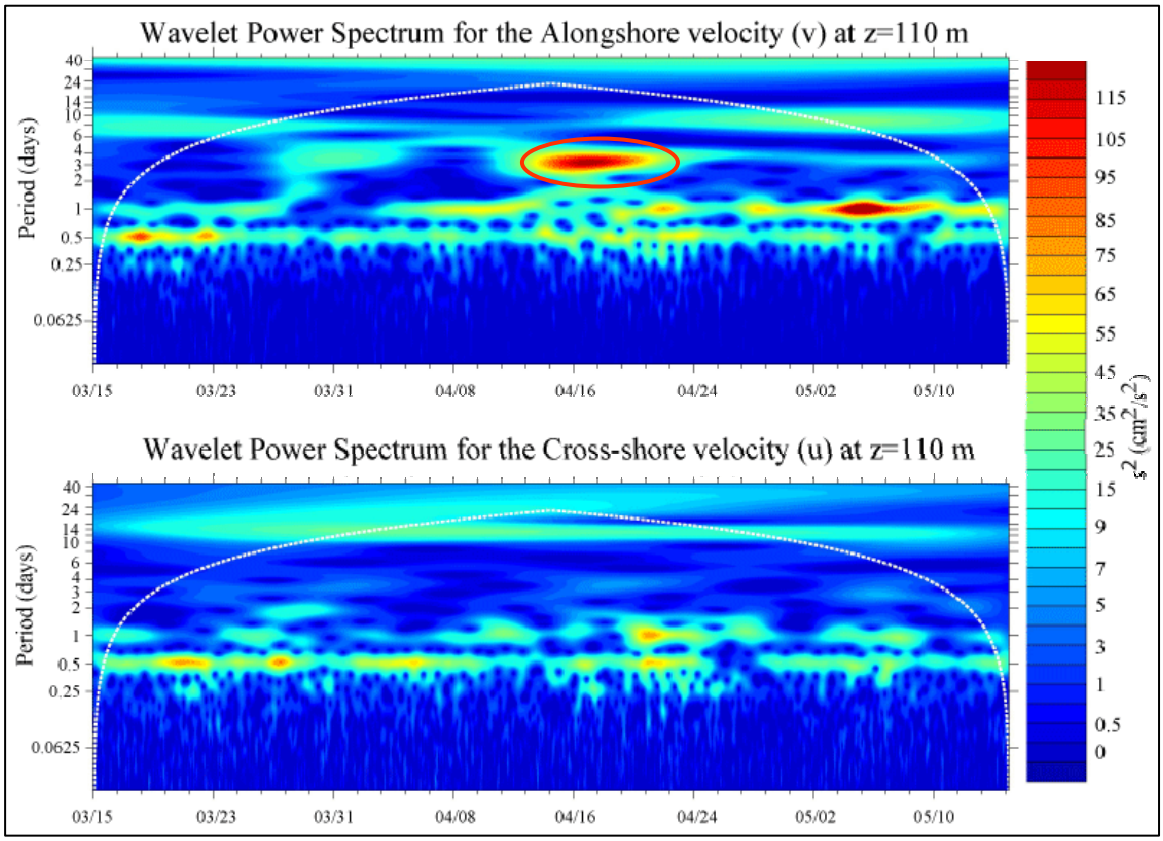

Figure III-32. Wavelet power spectra for the period: March 15 – May 15, 2007 at 110 m. Higher mode of energy at the 2-3 day period are circled in red (April event).

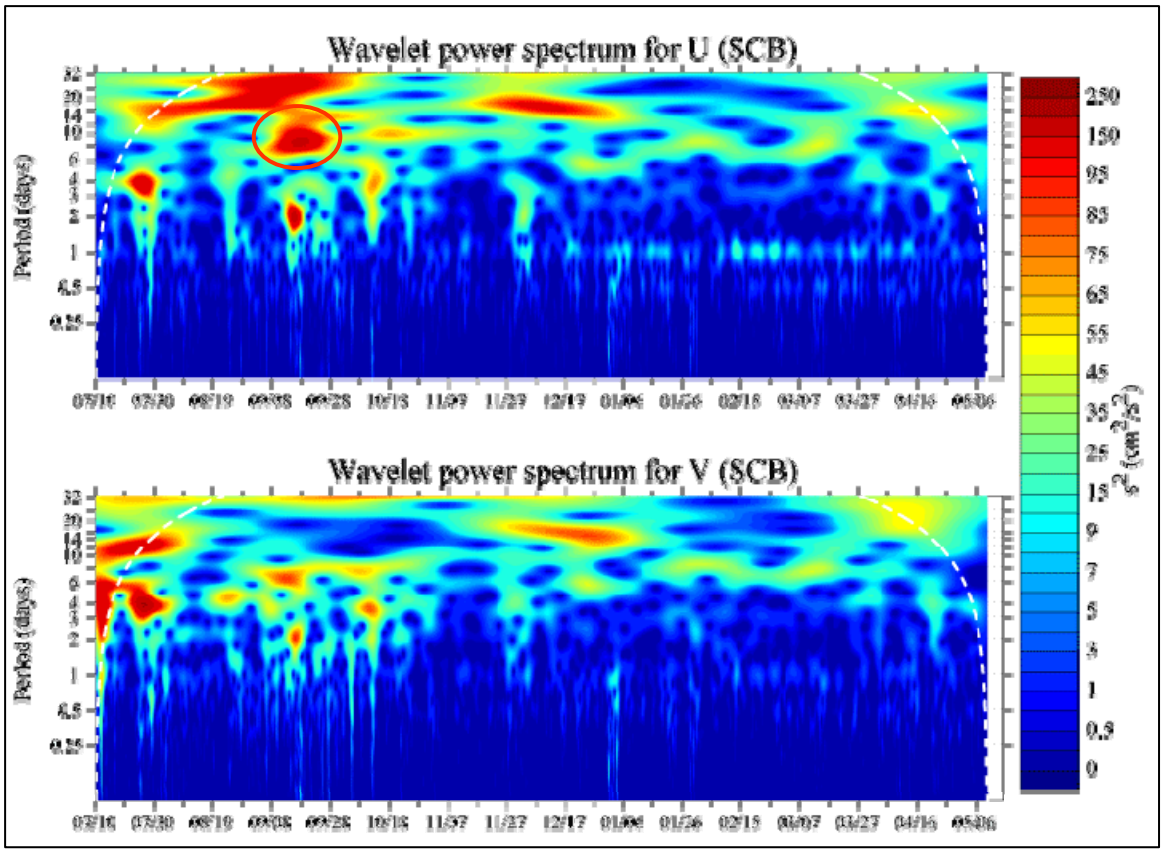

Figure III-33. Wind Stress wavelet power spectra for winds from NDBC - San Clemente Basin (SCB) buoy. Higher mode of energy at the 6-10 day period are circled in red.

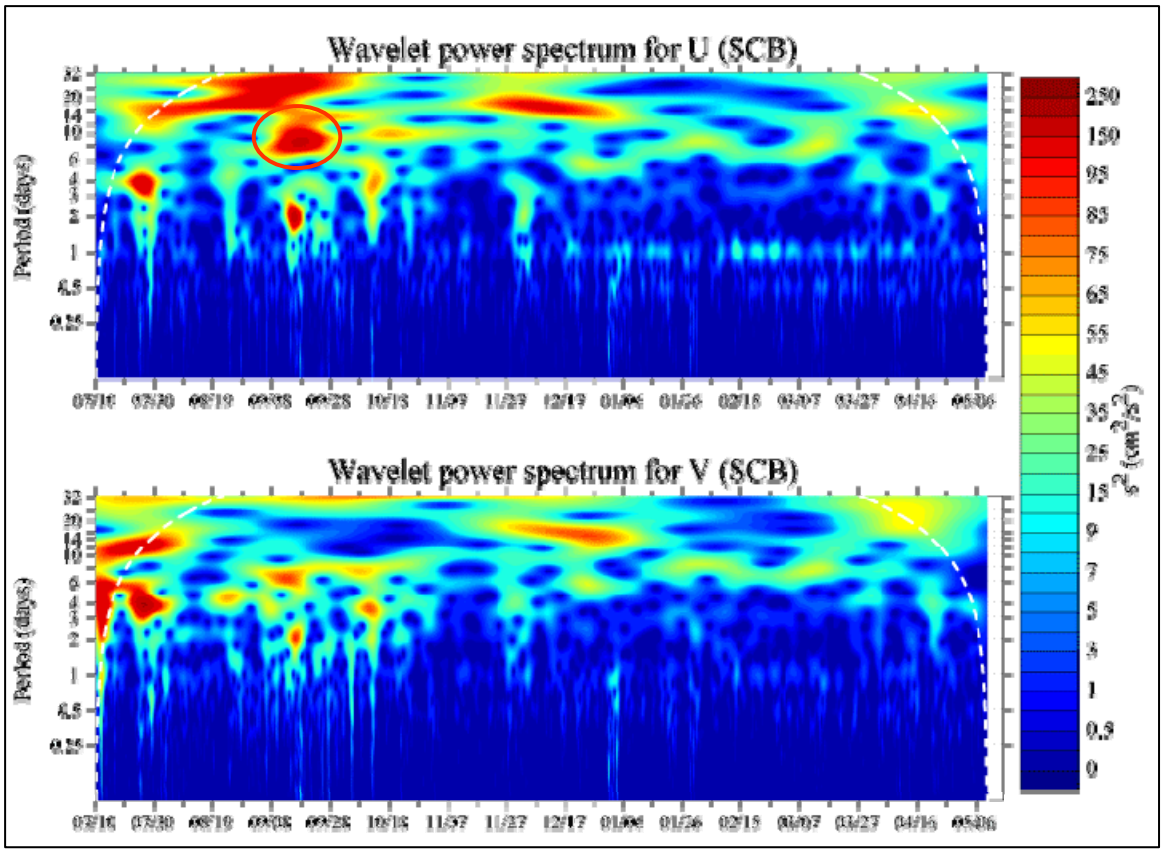

Figure III-34. Wind Stress wavelet power spectrum for winds from NDBC - Santa Monica Basin (SMB) buoy. Higher mode of energy at the 6-10 day period are circled in red.

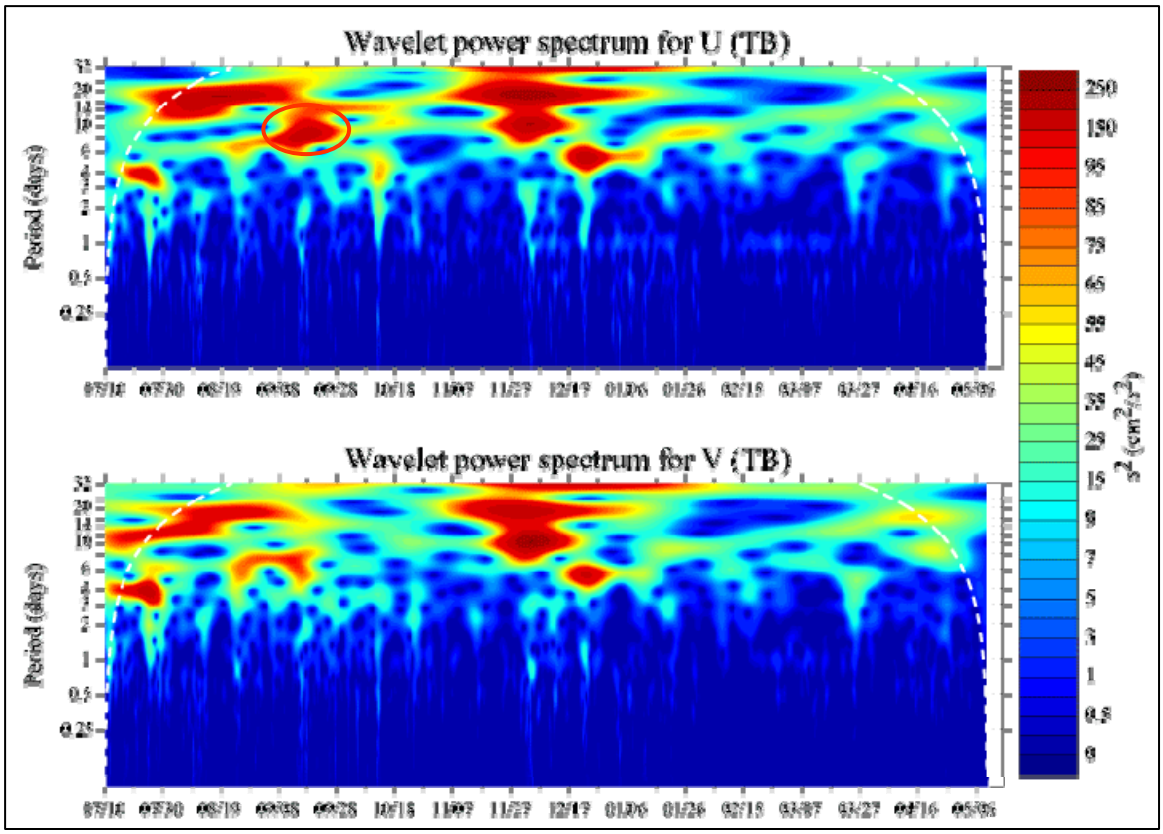

Figure III-35. Wind Stress wavelet power spectra for winds from NDBC – Tanner Banks (TB) buoy. Higher mode of energy at the 6-10 day period are circled in red.

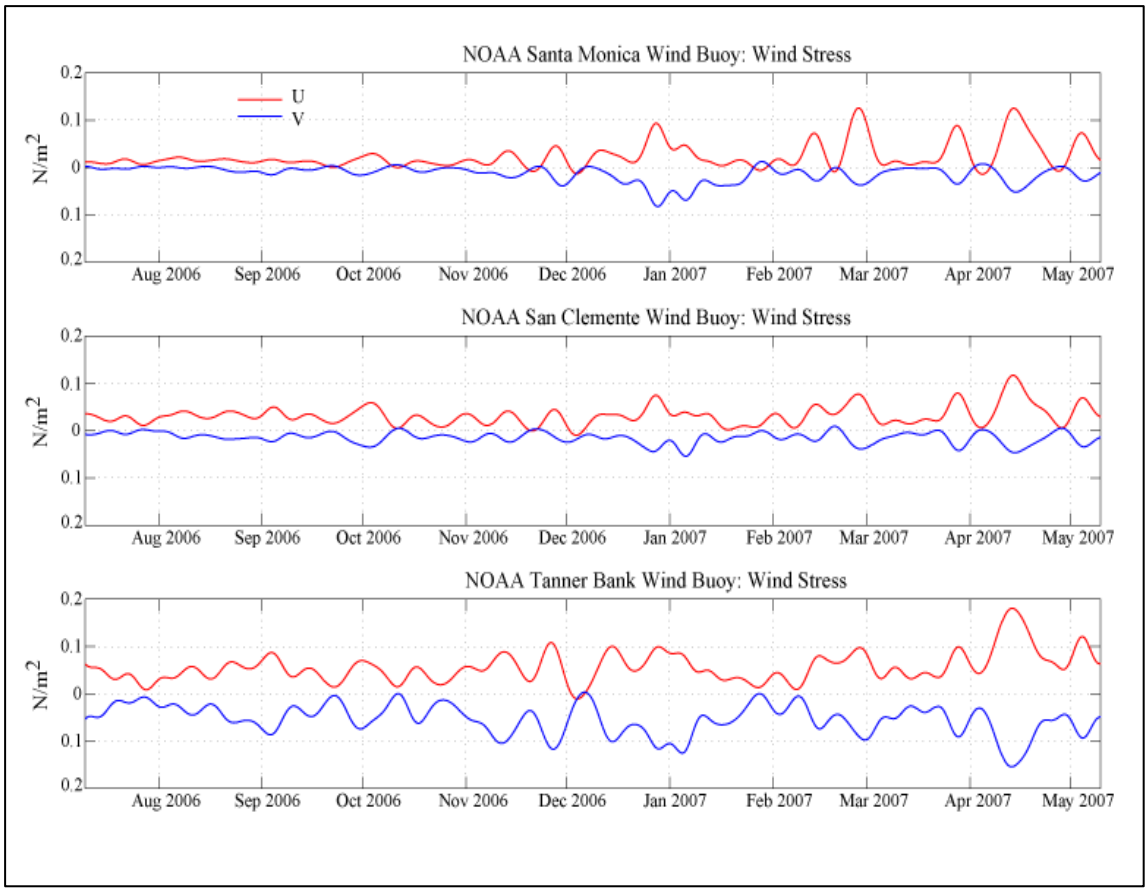

Figure III-36. Wind stress time-series for NDBC stations: 46025 – Santa Monica Basin, 46086 – San Clement Basin, and 46047 – Tanner Banks.

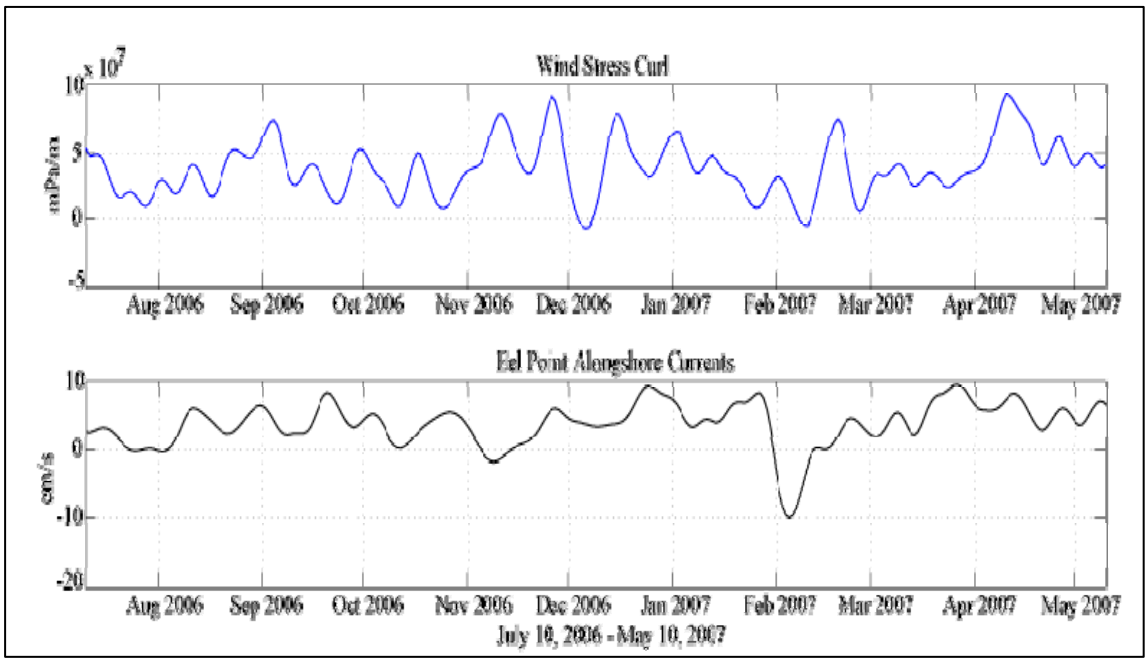

Figure III-37. Wind stress curl calculated between TB, SCB, and SMB NDBC stations, compared to the smoothed vertically averaged alongshore currents.

IV. SUMMARY OF RESULTS

This study was the first to describe the year-round current structure and stratification at Eel Point and is part of a continuing study. The currents around SCI were energetic and mostly dominated by semi-diurnal and diurnal tides. Periods of higher energy were observed, perhaps the most interesting of which was a ten day period in April, 2007. This chapter will summarize the important results from the study and place them in the context of other regional studies. Ocean currents and tides, seasonal variability of stratification, and forcing by wind stress and curl will be discussed.

A. OCEAN CURRENTS AT EEL POINT MOORING

Both the unsmoothed and smoothed currents were dominated by poleward flow along the isobaths with a mean (max) speed of 4 (50) cm/s. Occasional current reversals occurred that did not appear to be seasonal; on average 2-3 reversals occurred per season with the strongest reversal in the winter with observed equatorward maximum speed of 30 cm/s. In the summer the currents were relatively weak, with one significant (10 day) reversal in the cross-shore flow. In fall, currents remained relatively weak until mid-November when the poleward alongshore flow increased as did the eastward cross-shore flow. The winter currents were highly variable; alongshore currents were more strongly poleward than in the fall with the largest flow reversal at the beginning of February. The spring season had the strongest alongshore currents while the cross-shore flow was weak, with a mean flow of 1-2 cm/s.

There was only one other record of direct current measurements in San Nicholas basin for comparison with these results. In 1989, Tsai et al., (1990) measured the submesoscale current structure in San Nicholas Basin using synoptic shipboard current surveys during July 17-21 and September 2-6; the strongest currents they observed were poleward alongshore currents (mean flow 15 cm/s) on the eastern side of the basin, centered at 40-60 km to the west of SCI. These observations support the direction and magnitude of the currents reported here at Eel Point.

Next, seasonal variability of currents off Eel Point was compared to seasonal current variability observed at about the same latitude on the continental shelf offshore of Del Mar, California. The Del Mar observations were 3.6 km from shore in water about 65 m deep versus 5 km offshore of SCI in 135 m depth at Eel Point. The Del Mar current observations were made in the summer (July 27 to September 11, 1978), fall (October 21 to December 4, 1978), and winter December 21, 1978 to March 27, 1979) (Lentz and Winant, 1986). For this comparison, the rotated unsmoothed data were used, sorted into the same three seasons as in the Del Mar study, and a depth of 60 m was chosen.

Results are tabulated in Table 5. As expected, mean flow at both locations was along the isobaths. Weak poleward flow was observed at Del Mar during the summer (1.3 cm/s), weak equatorward flow observed in the fall (-1.1 cm/s), and a stronger equatorward flow observed in the winter (-6.8 cm/s). At Eel Point, the mean poleward flow was lowest in the summer (1.3 cm/s) and stronger in the fall (5.0 cm/s) and winter (5.9 cm/s). So, at 60 m, the currents were about the same at both locations in summer but as the year progressed, the current accelerated in opposite directions.

The standard deviation of the 60 m flow at Del Mar and Eel Point were about the same in summer, ~ 6 cm/s, but increased in fall and winter to ~ 10 cm/s at Eel Point, but remained ~6 cm/s at Del Mar. The standard deviation of the across shelf flow was much smaller at Del Mar because of the proximity of the current observation to the bottom.

B. SEASONAL VARIABILITY OF STRATIFICATION

As is typical for Eastern Boundary regions, stratification was minimum in summer and maximum in October. In July, the minimum temperature difference between 50 m and 129 m was observed (1.2˚ C) and maximum temperature difference between these depths was 4.5˚ C in October. The temperature change between 50 m and 91 m was about twice that observed between 91 m and 129 m. Salinity increased with depth so it added to the stratification. The maximum salinity difference between 50 m and 129 m was $\Delta S=0.5$ and occurred in July 2006 and the minimum salinity difference was $\Delta S=0.3$ in April 2007. The salinity change was about the same between 50 and 91 m as between 91 m and 129 m.

At all depths, maximum salinity and minimum temperatures were observed in July 2007, and minimum salinity in October 2006 and maximum temperature in February 2007. The July events were probably related to seasonal upwelling and it was noted that the subsurface temperature minimums occurred about 3-4 months later at Eel Point than the surface temperature minimums at inshore locations, e.g. NOAA Buoy 46025 (Catalina Ridge, CA) (Goericke et al., 2007). Minimum subsurface salinity in the region should be correlated with the onshore flow in the Southern California eddy but the observed October minimum was at odds with the fall to winter occurrence of the Southern California eddy. This suggests that pycnocline displacements, (as opposed to changes of water mass properties on isopycnals) control the temporal variability of salinity in San Nicholas basin.

C. TIDAL RESULTS

The dominant tidal energy was found in the semi-diurnal and diurnal tidal energy bands. The KE spectra and band averaged KE spectra showed that the dominant energy was associated with the semi-diurnal and diurnal tides at all three depths (34 m, 74 m, and 110 m). Semi-diurnal was strongest at mid-depth and diurnal was strongest at the near bottom and near surface. Semi-diurnal tidal peaks were dominant at all depths in the rotary spectra, followed by diurnal peaks. Inertial energy was observed at the near surface and near bottom depths in the rotary spectra.

The unsmoothed vertically averaged currents were dominated by semi-diurnal and diurnal tides (barotropic tidal currents). Semi-diurnal and diurnal modes were the dominant energy observed in the baroclinic tidal currents. In the (2 month) wavelet power spectra (which used the baroclinic tidal currents), there were strong pulses of energy in the near inertial/diurnal along and cross-shore currents that was only observed at the near surface depth. Intermittent pulses of higher energy at the near-inertial/diurnal and semi-diurnal periods energy in the along and cross-shore and rotary wavelet spectra were also observed. The amplitude of these pulses increased with depth so the near bottom had the highest energy associated with the near inertial/diurnal and semi-diurnal currents.

The amplitude of the semi-diurnal baroclinic currents at Eel Point did not track with the spring/neap cycles. Lerczak, (2000) studied the internal waves on the continental shelf near Mission Beach, California located at 32.75˚ N latitude (Eel Point mooring is located at 32.92˚ N latitude), and also found that semi-diurnal currents on the shelf were intermittent and did not follow the spring/neap cycle of the barotropic tides. Lerczak, (2000) also found intermittent diurnal currents which were driven by a persistent sea breeze that occurred off the coast of southern California. The intermittent diurnal currents observed at Eel Point could not be linked to the winds observed at regional NOAA buoys.

D. APRIL (OSCILLATION) EVENT

In April 2007, the alongshore flow oscillated with a 2-3 day period for approximately 10 days. These oscillations propagated downward through the water column with a vertical phase velocity of ~0.12 cm/s and maximum alongshore velocity (30 cm/s) occurred at the mid-depths. This event was not observed in the cross-shore velocity. This oscillation was not observed near the surface (34 m). The clockwise wavelet spectrum had high energy at 2 days decreasing to 1 day (near inertial/diurnal period); at this time the counterclockwise wavelet spectrum had a very weak pulse of energy. At mid-depth (74 m), the highest energy was observed and the clockwise and counterclockwise energy were equal, confirming that the flow was rectilinear alongshore. Near the bottom (110 m), the counterclockwise energy was dominant over the clockwise energy, so the horizontal currents were rotating counterclockwise.

During the period of these current oscillations in April, there was no energy observed in the wind stress wavelet spectra at any of the three buoy stations. The April event was therefore not induced by the regional wind stress.

E. WIND STRESS AND CURL

Wind stress within the bight is weak in comparison of wind stress north of Point Conception (Hickey, 1998). A 10-year time-series (Dorman and Winant, 1995; Winant and Dorman, 1997) showed the bight was sheltered from strong wind forcing throughout

the year. Wind stresses calculated from the SMB buoy and SCB buoy were relatively weak in comparison to the TB buoy, because SMB and SCB are within the bight and TB is on the western edge of the bight in the open ocean. Wind stress at all three buoys was strongest in April which was consistent with previous wind stress studies in the Southern California Bight (Winant and Dorman, 1997, Hickey, 1998, and Bray et al., 1999). During summer 2006 to summer 2007, the summer and fall wind stress at SMB and SCB were weaker than in the winter and spring. Winant and Dorman (1997) found that the wind stress tapers off in the summer and fluctuates in the winter due to propagating cyclones and anticyclones in the bight.

The wind stress curl was compared to the alongshore currents to see if curl was the forcing the current reversals observed throughout the time-series. The cross correlation between the wind stress curl and the alongshore currents indicated that there was no statistical relationship between the current reversals and wind stress curl. In Bray et al. (1999), the correspondence between the current transport and either wind stress or wind stress curl was found to be not particularly good, except in the spring when the equatorward anomalies in transport near the coast were associated with equatorward wind stress anomalies. The coastal upwelling event observed at Eel Point was unrelated to the wind stress or the wind stress curl obtained from regional NOAA buoys.

F. SIMPLE SLAB MODEL

Near inertial/diurnal energy was observed in the ocean currents throughout the July 2006 to July 2007 time period. Since the frequency resolution of the wavelet spectra was too coarse to distinguish between diurnal or inertial currents, it was not possible to discern when the inertial motion actually occurred. Demodulated inertial/diurnal currents at 34 m peaked on April 4, 2007. However, the near inertial currents were not predicted at this time using a slab model driven by SCB buoy wind stress. The model was run with the demodulated currents from 38 m and showed that near inertial energy was confined to the near surface (shallower than 38 m). So, although it was possible to have near inertial frequency oscillations at the surface that did not penetrate down through the mixed layer, this could not be verified using the Eel Point observations because the shallowest

observed currents were below the speculated mixed layer. Note too that the winds used in the model were from a regional NOAA buoy and were not local winds.

Table 5. Alonghore (AS) and cross-shore (CS) component of velocity for the currents off Del Mar, California and ***Eel Point, SCI.*** AS is positive toward 335˚ T ***(325˚T)*** and CS positive toward 65˚ T ***(55˚T).***

Season	Depth (m)	AS (cm/s)	CS (cm/s)	Standard Deviation - AS (cm/s)	Standard Deviation - CS (cm/s)	Principal axis orientation (deg T)
Summer	60	1.3	0.5	6	0.8	335
Summer	***62***	***0.9***	***-2.8***	***7.1***	***6***	***325***
Fall	60	-1.1	0.2	10.4	1.6	340
Fall	***62***	***5***	***-0.4***	***10***	***6***	***327***
Winter	60	-6.8	0.1	12.2	1	336
Winter	***62***	***5.9***	***0.6***	***10.8***	***6.6***	***328***

THIS PAGE INTENTIONALLY LEFT BLANK

V. CONCLUSION AND FUTURE RECOMMENDATIONS

The kinetic energy of the poleward flow along the coast off Eel Point was dominated by the clockwise rotating diurnal and semi-diurnal tidal variability. There were current flow reversals of low frequency flow observed each season, which were unrelated to regional wind stress and wind stress curl. There were also 2-3 and 3-4 day patterns of oscillations observed in the current velocity and stratification that were unrelated to regional wind stress and wind stress curl. Rotary spectra also revealed that there were dominant peaks of inertial energy at the near surface and near bottom depths. Wavelet power spectra were used to decompose the baroclinic tidal currents and revealed there were dominant modes of energy at the semi-diurnal and near inertial/diurnal period and that the strongest energy observed was at near the bottom.

In April 2007, an oscillatory event was observed in the alongshore currents and temperature and salinity time-series. It was observed at the mid-depth downward through to near bottom depths in the alongshore velocity field. The disturbance had a dominant poleward flow with maximum velocity (30 cm/s) observed at mid-depth and a vertical phase velocity of 0.12 cm/s. These oscillations were rectilinear at mid-water and became counterclockwise with depth. It was speculated that this event may have been a coastally trapped wave.

The wind stress within the bight was relatively weak throughout the time-series. Comparing the wind stress power spectra with along and cross-shore power spectra of the ocean currents, at the longer 6-10 day period observed in mid-November, there appeared to be some overlapping energy in both spectra. However, there was very little or no observed energy in the near inertial/diurnal and semi-diurnal or in the 2-3 day period in the wind stress power spectra that could be linked to the energy in the alongshore and cross-shore power spectra. There was no correlation between the wind stress curl and the alongshore currents. In conclusion, the wind stress and wind stress curl used in this study were not statistically correlated with the currents. Since there were no continuous local wind data available from SCI, the possibility of local (vs. regional) wind forcing could not be eliminated.

A. NAVAL RELEVANCE

Current and future naval operations are focused on coastal/littoral regions around the world and often depend upon knowledge of local ocean conditions. Surprisingly, there is little known about the currents and circulation patterns around SCI. SCI/SCORE is owned and operated by Navy and supports training for the largest concentration of naval forces in the world. SCI/SCORE creates a realistic environment for tactical readiness training for military units and personnel as they deploy overseas. This thesis provides information on ocean currents and stratification on the continental shelf at SCI for SCORE and military participants to use with military exercises, regional climatologies, ocean engineering design studies, and marine mammal studies. Ocean current information is needed in all amphibious assault operations, mine hunting exercises, search and rescue (SAR), and special operations. The current and stratification descriptions are useful for all ASW operations. It is crucial when planning any operation, whether training or for war to have the environmental information for the operating area. This ocean data from Eel Point are meant to provide such data to operating naval forces.

B. FUTURE RECOMMENDATIONS

Obtaining local wind data closer to or at the mooring would help explain or establish the role of local wind forcing. Deploying another mooring at the southern end of SCI would allow the alongshore pressure gradient to be estimated. These measurements of pressure gradients could help explain the current accelerations and classify the physical character of observed waves. Since these observations will continue to July 2008, it may be possible that another year of current and temperature/salinity time-series can be used to see if the July 2006 to July 2007 period described here was typical. It would be beneficial to compare the currents to those produced by a local numerical ocean model such as ROMs Nowcast: http://ourocean.pl.nasa.gov/SCB. Finally, it would be useful to compare the variability of physical conditions observed at Eel Point with marine mammal vocalizations recorded near the moorings.

LIST OF REFERENCES

Bray, N. A., A. Keyes, and W. M. L. Morawitz, The California Current system in the Southern California Bight and the Santa Barbara Channel, *J. Geophys. Res.*, *104*, C4, 7695–7714, 1999.

Craig, P. D., A model of diurnally forced vertical current structure near 30˚ latitude, *Cont. Shelf Res*., 9, (No.11), 965-980, 1989.

Department of Navy. 2005. Marine Resources Assessment for the SOCAL OPAREA. Pacific Division, Naval Facilites Engineering Command, Pearl Harbor Hawii.

Dorman, C. E., and C. D. Winant, Buoy observations of the atmosphere along the west coast of the United States, 1981-1990, *J. Geophys. Res.,* 100(C8), 16,029-16,044, 1995.

Emery, W.J., and R.E. Thomson, Data Analysis Methods in Physical Oceanography. Kentucky: Gray publishing, 1997.

Gordon, L., Acoustic Doppler current profiler – Principles of operation: A practical primer: RDI Instruments, San Diego, CA, 1996.

Goericke, R. V., E. Koslow, T. Sydeman, W. J. Schwing, R. B. Bograd, S. J. Peterson, W. T. Emmett, R. Lara, and J. R. L. Castro, J. G. Valdez, K. D. Hyrenbach, R. W. Bradley, M. J. Weise, J. T Harvey, C. Collins, and N. C. H. Lo, The state of the California Current, 2006-2007: Regional and Local Processes Dominate, CalCOFI Rep., Vol. 48, 33-66, 2007.

Hickey, B.M., Coastal oceanography of western North America from the tip of Baja California to Vancouver Island, in *The Sea: The Global Costal Ocean: Regional Studies and Syntheses*, vol. 11, edited by A.R. Robinson and K.H. Brink, chap. 12, pp. 345-393, 1998.

Hickey, B.M., E.L. Dobbins, and S.E. Allen, Local and remote forcing of currents and temperature in the central southern California bight, *J. Geophys. Res*., in press, 2003.

Hickey, B.M, The California Current System – hypothesis and facts, *Prog. Oceanogr*., 8. pp. 191-279, 1979.

Hickey, B.M., and N. E. Pola, The seasonal alongshore pressure gradient on the west coast of the United States, *J. Geophys. Res*., 88(C12), 7623-7633, 1983.

Huyer, A.., P. M. Kosro, S. J. Lentz, and R. C. Beardsley, Poleward flow in the CCS, in *poleward Flows along Eastern Oceanic Boundaries*, Coastal and Estuarine Studies, No. 34, 142-156, Springer-Verlag, New York Inc., 1989.

Large, W.G., and S. Pond, Open Ocean Momentum Flux Measurements in Moderate to Strong Winds, *J. Phys. Oceanogr.,* 11, 324-336, 1981.

Lentz, S. L., and C. D. Winant, Subinertial Currents on the Southern California Shelf, *J. Phys. Oceanogr.,* 16, 1737-1750, 1986,

Lerczak, J. A., Internal Waves on the Southern California Shelf, UCSD Dissertation, 2000.

Lynn, R. J., and J.J. Simpson, The Flow of the Undercurrent over the Continental Borderland off Southern California, *J. Geophys. Res.*, *95,* C8, 12,995-13008, 1990.

Lynn, R. J., and J. J. Simpson, The California Current System: The seasonal variability of its physical characteristics, *J. Phys. Oceanogr.,* 92(C12), 12,947-12,966, 1987.

Paduan, J. D., R. A. De Szoeke, and R. A. Weller, Inerial Oscillations in the Upper Ocean During the Mixed Layer Dynamics Experiment (MILDEX) , *J. Geophys. Res.*, 94, C4, 4835-4842, 1989.

Pawlowicz, R., B. Beardsley, and S. Lentz. Classical Tidal Harmonic Analysis Including Error Estimates in MATLAB® using T_TIDE. *Computers and Geosciences* 28, 929-937, 2002.

Pollard, R. T., and R. C. Millaard, Comparison between observed and simulated wind-generated inertial oscillations, *Deep Sea Res.,17*, 813-821, 1970.

Simpson, M. R., Discharge Measurements Using a Broad-Band Acoustic Doppler Current Profiler, United States Geological Survey, Sacramento, CA, 2001.

Torrence, C., and G. P. Compo, A practical guide to wavelet analysis, *Bull Amer. Met. Soc.,* 79 (1), 61-78, 1998.

Tsai, C. M., P. F. Jessen, P. C. Chu, and C. A. Collins, Submesoscale structure of the California Current near San Clemente Island, NPS Tech. Rpt, 68-90-003, April 1990.

Winant, C. D., and C. E. Dorman, Seasonal patterns of surface wind stress and heat flux over the Southern California Bight, *J. Geophys. Res., 102, C3,* 5,641-5,653, 1997.

THIS PAGE INTENTIONALLY LEFT BLANK

INITIAL DISTRIBUTION LIST

1. Defense Technical Information Center
   Ft. Belvoir, VA

2. Dudley Knox Library
   Naval Postgraduate School
   Monterey, CA

3. Navy Oceanographic Office
   Balch Boulevard
   Stennis Space Center

4. Mary L. Batteen
   Naval Postgraduate School
   Monterey, CA

5. Curtis A. Collins
   Naval Postgraduate School
   Monterey, CA

6. Fred L. Bahr
   Naval Postgraduate School
   Monterey, CA

7. Erin Oleson
   Scripps Institution of Oceanography
   University of California
   La Jolla, CA

8. John Hildebrand
   Scripps Institution of Oceanography
   University of California
   La Jolla, CA

9. Thomas A. Rago
   Naval Postgraduate School
   Monterey, CA

10. Tetyana Margolina
    Naval Postgraduate School
    Monterey, CA

11. Marla D. Stone
Naval Postgraduate School
Monterey, CA

12. John Joseph
Naval Postgraduate School
Monterey, CA

13. Frank Stone
N45
Washington, D.C.

14. Dale Liechty
N45
Washington, D.C.

15. LCDR Mike Loomis
Naval Postgraduate School
Monterey, CA

16. LTJG Jessica Mohamed
Naval Postgraduate School
Monterey, CA

17. LT Christian Jensen
Naval Postgraduate School
Monterey, CA

18. Professor Jeffery D. Paduan
Naval Postgraduate School
Monterey, CA

19. Jenny Marshall
Naval Facilities Engineering Command, Pacific
San Diego, CA

20. Robert Tahmic
NAS North Island
San Diego, CA

21. Heidi Nevitt
NAS North Island
San Diego, CA

22. Professor Clive Dorman
Scripps Institution of Oceanography
University of California
La Jolla, CA

23. Professor Clinton Winant
Scripps Institution of Oceanography
University of California
La Jolla, CA

24. Professor Libe Washburn
University of California
Santa Barbara, CA

25. CDR Ashley Evans,
Commanding Officer
SGOT, NAS North Island
San Diego, CA

26. Carl Szczechowski
Naval Oceanographic Office
Stennis Space Center, MS

27. CAPT. Ernie Young, USN (ret)
N45
Washington, D.C.